The IQGAP1-hnRNPM interaction links tumour-promoting alternative splicing to heat-induced signals

Andrada Birladeanu[1,‡], Malgorzata Rogalska[2,‡], Myrto Potiri[1,‡], Vassiliki Papadaki[1], Margarita Andreadou[1], Dimitris Kontoyiannis[1,3], Zoi Erpapazoglou[1], Joe D. Lewis[4], Panagiota Kafasla[*,1]

[1]Institute for Fundamental Biomedical Research, B.S.R.C. "Alexander Fleming", 34 Fleming st., 16672 Vari, Athens, Greece

[2]Centre de Regulació Genòmica, The Barcelona Institute of Science and Technology and Universitat Pompeu Fabra, Dr. Aiguader 88, 08003, Barcelona, Spain

[3]Department of Biology, Aristotle University of Thessaloniki, Greece

[4]European Molecular Biology Laboratory, 69117 Heidelberg, Germany

[‡]These authors contributed equally to this work

[*]Correspondence: kafasla@fleming.gr

Abstract (150 words):

Alternative Splicing (AS) is extensively regulated during the cell cycle and is also involved in the progression of distinct cell cycle phases. Stressing agents, such as heat shock, halts AS affecting mainly post-transcriptionally spliced genes. Stress-dependent regulation of AS relies possibly on the subnuclear location of its determinants, such us Serine-Arginine rich (SR) and heterogeneous nuclear ribonucleoproteins, hnRNPs.

Spliceosomal components like SRSF1, SRSF9, SRp38, hnRNPM have been connected to such responses of AS, but how they are directed to respond to stress remains largely unknown. Here, we report that upon heat stress, the cytosolic scaffold protein IQGAP1 translocates into the nucleus of gastric cancer cells, where it acts as a tethering module for hnRNPM and other spliceosome components, mediating their subnuclear positioning and their response to stress. Moreover, together, they regulate the AS of the anaphase promoting complex (ANAPC) subunit 10 to promote gastric cancer cell growth.

Introduction

In humans, more than 95% of multi-exonic genes are potentially alternatively spliced[1,2]. Precise modulation of Alternative Splicing (AS) is essential for shaping the proteome of any given cell and altered physiological conditions can change cellular function via AS reprogramming[3]. The importance of accurate AS in health and disease, including cancer[4–7], has been well documented. However, evidence connecting AS regulation to signalling comes mostly from few cases where localization, expression, or post-translational modifications of specific splicing factors such as Serine-Arginine-rich (SR) proteins or heterogeneous nuclear ribonucleoproteins (hnRNPs)[3,8] are altered.

An abundant, mainly nuclear protein of the hnRNP family is hnRNPM, with four isoforms that arise from AS and/or post-translational modifications[9]. The only nuclear role so far reported for hnRNPM is in spliceosome assembly and splicing itself[10,11], including regulation of AS of other as well as its own pre-mRNAs[12–14]. The association of hnRNPM with the spliceosome is abolished under heat-induced stress[11,15], known to affect largely post-transcriptional splicing events[16], suggesting hnRNPM's response in stress-related signalling pathways.

HnRNPM-regulated AS events have been linked to disease development and progression. Specifically, hnRNPM-mediated AS is deterministic for the metastatic potential of breast cancer cells, due to cell-type specific interactions with other splicing factors[17–19]. Furthermore, in Ewing sarcoma cells, hnRNPM abundance and subnuclear localization change in response to a chemotherapeutic inhibitor of the PI3K/mTOR pathway, resulting in measurable AS changes[20]. Very recently, hnRNPM was shown to respond to pattern recognition receptor signalling, by modulating the AS outcome of an RNA-regulon of innate immune transcripts in macrophages[21].

Despite such growing evidence on the cross-talk between hnRNPM-dependent AS and cellular signalling, how distinct signals are transduced to hnRNPM and the splicing machinery remains unclear. Here, we present conclusive evidence of how this could be achieved. We describe a novel interaction between hnRNPM and the scaffold protein IQGAP1 (IQ Motif Containing GTPase Activating Protein 1) in the nucleus of gastric cancer cells. Cytoplasmic IQGAP1 acts as a signal integrator in a number of signalling pathways[22], but there is no defined role for the nuclear pool of IQGAP1. With *IQGAP1* mRNA being overexpressed in many malignant cell types, the protein seems to regulate cancer growth and metastatic potential[23–25]. Moreover, aged mice lacking IQGAP1 develop gastric hyperplasia suggesting an important *in vivo* role for IQGAP1 in maintaining the gastric epithelium[26]. In the present study we show that this novel, nuclear interaction between hnRNPM and IQGAP1 links heat-induced signals to hnRNPM-regulated AS in gastric cancer, a cancer type that has been associated with a significantly high incidence of AS changes[6,7]. Additionally, we show that depletion of both interacting proteins results in alternative splicing changes that disfavour tumour growth, which makes them and their interaction interesting cancer drug targets.

Results

hnRNPM and IQGAP1 expression levels are significantly altered in gastric cancer.

Analysis of the hnRNPM and IQGAP1 protein levels by immunofluorescence on commercial tissue microarrays revealed increased hnRNPM and IQGAP1 staining in tumour as compared to normal tissue, especially in adenocarcinoma samples **(Fig. 1a and Supplementary Fig. 1a-c).** This agrees with TCGA data analysis indicating significantly increased expression of both *IQGAP1* and *hnRNPM* mRNAs in stomach adenocarcinoma (STAD) vs normal tissue samples (**Fig. 1b**). Furthermore, a strong correlation between the expression of the two mRNAs (*HNRNPM* and *IQGAP1*) in normal tissues (GTex) was revealed, which was reduced in normal adjacent tissues (Normal) and eliminated in STAD tumours (**Fig. 1c**).

Detection of hnRNPM and IQGAP1 protein levels in a number of gastric cancer cell lines by immunoblotting (**Fig. 1d**) identified cell lines with similar levels of hnRNPM and low (MKN45, AGS) or high (NUGC4, KATOIII) levels of IQGAP1, corroborating the TCGA data. Two of those STAD cell lines were used for further studies on the interaction between hnRNPM and IQGAP1 (NUGC4 and MKN45) since they have similar hnRNPM, but different IQGAP1 levels.

IQGAP1 and hnRNPM regulate gastric cancer cell growth *in vitro* and *in vivo*

To test the significance of IQGAP1 and hnRNPM in tumour development, we used a CRISPR-Cas9 approach to generate *hnRNPM*-KnockOut (KO) cell lines, *IQGAP1*^{KO} and double KO. We knocked-out successfully *IQGAP1* in both MKN45 and NUGC4 cells without significant change in hnRNPM protein levels (**Supplementary Fig. 2a**). However, numerous attempts to disrupt the ORF of hnRNPM resulted in ~75%

reduction, as we could not isolate single hnRNPM^{KO} clones. Thus, for the subsequent experiments we either worked with mixed cell populations (e.g. MKN45-*hnRNPM*^{KO}-*IQGAP1*^{KO}) with 75% reduced hnRNPM expression levels (**Supplementary Fig. 2a**), or, where stated, we used siRNAs for down-regulation of the hnRNPM levels.

To evaluate the role of the two proteins in gastric cancer progression, we first assayed the STAD cell lines and the derivative KO/Knock-Down cell lines for their metabolic activity (**Fig. 2a**). Downregulation of hnRNPM alone or in combination with IQGAP1 impairs cellular metabolic activity, compared to the parental lines, as indicated by MTT assays performed over a period of 5 days. Interestingly, we detected an increased metabolic rate in IQGAP1^{KO} cells, which can be attributed to hnRNPM-independent changes in metabolic activity in the absence of IQGAP1 (data not shown). In a 2D colony formation assay, cells with reduced levels of both IQGAP1 and hnRNPM proteins generated a significantly reduced number of colonies compared to parental cells (**Fig. 2b**). Furthermore, cell cycle analyses using propidium iodide combined with flow cytometry showed that unsynchronized IQGAP1^{KO} cells depicted a small but significant increase of cell population at the S and G2/M phases with subsequent reduction of G1 cells (**Fig. 2c**). hnRNPM^{KO} cells showed a similar phenotype, whereas depletion of both interacting proteins (hnRNPM^{KO}-IQGAP1^{KO}) enhanced the effect (**Fig. 2c**). These differences were stronger after cell synchronization (**Supplementary Fig. 2b**). Wound healing assays did not reveal significant differences in the migratory ability of these cell lines, only an increase in wound healing rate for hnRNPM^{KO} cells compared to the parental line. Importantly, this expedited wound healing in hnRNPM^{KO} cells was completely abolished upon concomitant absence of IQGAP1 (**Supplementary Fig. 2c**).

To examine the *in vivo* effect of abrogating IQGAP1 and hnRNPM on tumour development and progression, we injected MKN45, MKN45-*IQGAP1*^{KO}, MKN45-*hnRNPM*^{KO} and MKN45-*hnRNPMKO-IQGAP1*^{KO} cells subcutaneously into the flanks of NOD/SCID mice. Measurements of tumour dimensions throughout the experiment demonstrated that cells lacking both IQGAP1 and hnRNPM result in significantly reduced tumour growth compared to the parental and the single KO cells **(Fig. 2d**). Immunohistochemical analysis of the tumours confirmed greatly reduced levels of hnRNPM and/or IQGAP1 in the mutant cell line-derived xenografts. Furthermore, Ki-67 staining was significantly reduced in the single and double KO tumours compared to the parental cell line-derived ones, showing the involvement of the two proteins in the *in vivo* proliferation of gastric cancer cells (**Fig. 2e**). Collectively, these results demonstrate that co-operation of IQGAP1 and hnRNPM is required for gastric cancer cell growth and progression both *in vitro* and *in vivo*.

IQGAP1 and hnRNPM interact in the nucleus of gastric cancer cell lines

An interaction between hnRNPM and IQGAP1 was detected in nuclear extracts from both STAD cell lines using immunoprecipitation with anti-IQGAP1 antibodies (**Fig. 3a**). Treatment with RNaseA showed that the two proteins interact independently of the presence of RNA. This interaction also appeared to be DNA-independent (**Supplementary Fig. 3a)**. Immunoprecipitation using anti-IQGAP1 antibodies from cytoplasmic extracts did not reveal interaction with the minor amounts of cytoplasmic hnRNPM (**Supplementary Fig. 3b and data not shown)**, indicating that if the proteins do interact in the cytoplasm, these complexes are less abundant compared to the nuclear ones.

In agreement with previous reports of a small fraction of IQGAP1 entering the nucleus in a cell cycle-dependent manner[27], we confirmed the presence of IQGAP1 in the nucleus of both NUGC4 and MKN45 cells using confocal imaging (**Fig. 3b**) The interaction of nuclear IQGAP1 with hnRNPM *in situ* was confirmed using proximity ligation assays (PLA) (**Fig. 3c).** Quantification of the PLA signal per cell demonstrated that the interaction between the two proteins was clearly detectable in the nucleus of both cell lines (**Fig. 3d**). Some cytoplasmic interaction sites were also detected, but they were minor compared to the nuclear ones (**Fig. 3c, d**) in agreement with the immunoprecipitation results from cytoplasmic extracts (**Supplementary Fig. 3b**). Together these results demonstrate the RNA-independent, nuclear interaction between hnRNPM and IQGAP1 in gastric cancer cells.

Nuclear IQGAP1-containing RNPs are involved in splicing regulation

To identify other possible nuclear IQGAP1 interacting partners, we performed immunoprecipitation with anti-IQGAP1 Abs from nuclear extracts of NUGC4 cells and analysed the resulting proteins by LC-MS/MS (**Supplementary Table 1**). GO-term enrichment analysis of the co-precipitated proteins showed a significant enrichment in biological processes relevant to splicing regulation (**Supplementary Fig. 4a**). Construction of an IQGAP1 interaction network revealed that IQGAP1 can interact not only with the majority of the hnRNPs, but also with a large number of spliceosome components (mainly of U2, U5snRNPs) and RNA-modifying enzymes (**Fig. 4a**). The interactions between IQGAP1 and selected hnRNPs (A1, A2B1, C1C2, L, M) and with selected spliceosome components and RNA processing factors (SRSF1, CPSF6, DDX17, DHX9, ILF3/NF90)[28] were independently validated in both NUGC4 and MKN45 cells (**Fig. 4b, Supplementary Fig. 4b**). The interactions of IQGAP1 with

hnRNPs A1, A2B1 are RNA-dependent, whereas only a subset of hnRNPs (L, C1/C2) interact with IQGAP1 in the absence of RNA (**Fig. 4b**). These observations pinpointed to the RNA-independent interaction with hnRNPM as a distinct one, worthy of further investigation.

In the nuclear extracts used in our immunoprecipitations hnRNPM is enriched together with the majority of hnRNPs[29,30] (e.g. A2B1, K), other nuclear speckle components like SRSF1, and nuclear matrix associated proteins like SAFB and MATRIN3 (**Fig. 4c and Supplementary Fig. 4c**), but not histones such as H3, which are present mainly in the insoluble nuclear material (**Supplementary Fig. 4c**). To further explore the interactions of nuclear IQGAP1 with the splicing machinery, we queried whether itself and its interacting partners are present in described splicing-related subnuclear fractions[31]. This was justified by the recent identification of hnRNPM as a significant component of the Large Assembly of Spliceosome Regulators (LASR). This complex is assembled via protein-protein interactions, lacks DNA/RNA components, and appears to function in co-transcriptional AS[31]. In MKN45 cells, IQGAP1 and hnRNPM co-exist mainly in the soluble nuclear fraction together with hnRNPs K, C1/C2 and other spliceosome components[31]. Significantly smaller IQGAP1 and hnRNPM amounts were detected in the proteins released from the HMW material upon DNase treatment (D), together with hnRNPC1/C2 and other spliceosome components, including SF3B3 (**Supplementary Fig. 4d).** Thus, the interacting pools of IQGAP1 and hnRNPM are not major LASR components and possibly participate in post-transcriptional splicing events.

To assess the possible functional involvement of IQGAP1 in splicing, we used the hnRNPM responsive DUP51M1, DUP50M1 and control DUP51-ΔM and DUP50-ΔM mini-gene reporters[31]. DUP51M1 is a three exon minigene, where exon 2 contains a unique UGGUGGUG hnRNPM consensus binding motif that results in skipping of this

exon upon hnRNPM binding. The DUP51-ΔM minigene carries a mutation in the hnRNPM binding site, resulting in increased inclusion of exon 2[31]. The DUP50M1 reporter was derived from DUP51M1 by slightly altering the hnRNPM binding site on exon 2 (to UGUUGUGUUG). The DUP50-ΔM reporter has also a mutation in the hnRNPM binding site, that does not allow hnRNPM binding[31]. Transfection of the two gastric cancer cell lines with the pDUP51M1 plasmid and subsequent RT-PCR analysis with primers that allow detection of the two possible mRNA products, revealed different splicing patterns of the reporter: significantly more inclusion of exon 2 was detected in NUGC4, which express IQGAP1 at higher levels, than MKN45 (**Supplementary Fig. 4e)**. Moreover, analysis of the splicing pattern of the DUP51-ΔM reporter showed that the dependence of exon 2 inclusion on hnRNPM was more pronounced in MKN45 compared to NUGC4 (**Supplementary Fig. 4e)**. The same results were obtained when we used the DUP50M1 and DUP50ΔM sets of reporters. These results prompted us to focus on MKN45 cells to further probe the involvement of the hnRNPM-IQGAP1 interaction in AS. In the IQGAP1^{KO} cells, the DUP51M1 reporter presented a significant ~2-fold increase in exon 2 inclusion compared to the parental cells (**Fig. 4d)**. As expected from the interaction of IQGAP1 with other splicing factors, splicing of the DUP51-ΔM reporter was also affected upon IQGAP1 loss. However, this change was smaller (~1.3-fold increase) compared to the impact on hnRNPM-dependent splicing (**Fig. 4d**). Attempts to restore splicing efficiency by expressing GFP-IQGAP1 were inconclusive, as the recombinant protein localized very efficiently in the nucleus[27], thus inhibiting rather than rescuing exon 2 skipping (**Supplementary Fig. 4f**), likely due to sequestration of hnRNPM from the splicing machinery. These results denote that IQGAP1 interacts with a large number of splicing

factors, of which hnRNPM stands out as a unique, RNA-independent interaction, important for hnRNPM's activity in alternative splicing.

A broad role of IQGAP1 in hnRNPM-dependent alternative splicing

To determine whether IQGAP1^{KO} results in broad splicing deregulation, we profiled AS changes between MKN45 and MKN45-*IQGAP1^{KO}* cells by RNA-seq (**Fig. 5a-c)**. A number of significantly altered AS events were detected (**Fig. 5a** and **Supplementary Table 2a**) more than 50% of which were alternative exons (**Fig. 5b)**. Statistical analysis showed that down-regulated exons are more likely to have the hnRNPM binding motif than up-regulated exons (chi-square (1, 86) = 36.4848, $P < 0.00001$; **Fig. 5c, d**). The presence of hnRNPM consensus binding motifs[13] was significantly enriched downstream of 81% of the down-regulated alternative exons. GO term enrichment analysis of the affected genes yielded significant enrichment of the biological processes of cell cycle (GO:0007049, *P*: 3.75E-04) and cell division (GO:0051301, *P*: 3.33E-04) (**Supplementary Table 2b**), connecting these results to the detected cell cycle defects (**Fig. 2c**).

Splicing events selected for validation were required to adhere to most of the following criteria: 1) high difference in Psi (ΔPsi) between the two cell lines (where [Psi] is the Percent Spliced In, i.e. the ratio between reads including or excluding alternative exons), 2) involvement of the respective proteins in the cell cycle, 3) previous characterization of pre-mRNAs as hnRNPM targets[32,33] and/or 4) presence of the hnRNPM-consensus motif up- or downstream of the alternative exon. 12 out of 19 AS events (63%) selected based on the above criteria were validated by RT-PCR **(Fig. 5e, Supplementary Fig. 5a-c, Supplementary Table 3).** Therefore, the above indicate that IQGAP1 and hnRNPM co-regulate the AS of alternative exons in a cell-cycle-

related RNA regulon. Within this regulon, ANAPC10 pre-mRNA was singled out for further analysis as it had the highest change in |ΔPsi|/Psi combination (**Fig. 5a, e**) and it is an hnRNPM-eCLIP target[33] with the major hnRNPM binding sites downstream of the regulated exon, where the predicted hnRNPM consensus binding motif is also located (**Supplementary Fig. 5d**).

IQGAP1 and hnRNPM co-operatively regulate the function of APC/C through AS of the *ANAPC10* pre-mRNA

Importantly for cancer cells, ANAPC10 plays a crucial role in cell cycle and cell division[34–37] as a substrate recognition component of the anaphase promoting complex/cyclosome (APC/C), a cell cycle-regulated E3-ubiquitin ligase that controls progression through mitosis and the G1 phase of the cell cycle. ANAPC10 interacts with the co-factors CDC20 and/or CDH1 to recognize targets to be ubiquitinated and subsequently degraded by the proteasome. In *IQGAP1*^{KO} cells, increased levels of *ANAPC10* exon 4 skipping were detected and simultaneous knock-down of hnRNPM using siRNAs led to further increase in *ANAPC10* exon 4 skipping compared to scr-siRNA transfected cells (**Fig. 5e** and **6a**). Skipping of exon4 is predicted to result in the preferential production of an isoform lacking amino acid residues important for interaction with the D-box of the APC/C targets[36,37]. To verify that this is the case, using LC-MS/MS analyses of the proteomes of the parental and the *IQGAP1*^{KO} cell lines, we compared the levels of known targets of the APC/C complex. We detected increased abundance of anaphase-specific targets of the APC/C-CDH1 [35], namely RRM2, TPX2, ANLN, and TK1, but not of other APC/C known targets (**Supplementary Fig. 6a).** Immunoblotting showed that TPX2, RRM2 and TK1 levels were indeed increased in

IQGAP1^{KO} cells and even more after concomitant siRNA mediated *hnRNPM* knock-down (**Fig. 6b**). The same was true for CDH1/FZR, an APC/C co-factor, which is also a target of the complex, as is ANLN (**Supplementary Fig. 6b**). Interestingly, ANAPC10 levels were reduced in the *IQGAP1*^{KO} cells after knock-down of *hnRNPM*.

Given the role of APC/C and its targets, TK1, RRM2 and TPX2 in the progression of mitosis and cell division[35,38–40], we determined the impact of the downregulation of both *IQGAP1* and *hnRNPM* on cell division. Using DAPI staining and anti-β-tubulin cytoskeleton immunostaining we detected a significant number of double *IQGAP1-hnRNPM*^{KO} cells being multinucleated (2 or more nuclei; **Fig. 6d-e**). A similar phenotype was detected when we used siRNAs to downregulate hnRNPM levels (**Supplementary Fig. 6c**). These results denote that IQGAP1 interacts with hnRNPM in the nucleus of gastric cancer cells and co-operatively they generate at least an alternatively spliced isoform of ANAPC10. This, in turn, tags cell cycle-promoting proteins for degradation, thus contributing to the accelerated proliferation phenotype of tumour cells.

IQGAP1 alters hnRNPM's ability to respond to heat-shock in cancer cells

To detect the mechanism behind the IQGAP1-hnRNPM co-regulation of AS events, we investigated whether binding of hnRNPM on its pre-mRNA target is altered in the absence of IQGAP1. For this, we used the previously mentioned minigene reporter and tested the association of hnRNPM with the DUP51M1 transcript using crosslinking, immunoprecipitation with anti-hnRNPM antibodies, and RT-PCR of the associated pre-mRNA. No significant differences were detected between the parental and the *IQGAP1*^{KO} cells in the amount of RNA that was crosslinked to hnRNPM

(**Supplementary Fig. 7a**), indicating that IQGAP1 does not regulate the binding of hnRNPM to its RNA targets.

The activity of hnRNPM in splicing is altered upon heat-shock, when hnRNPM is shifted from the nucleoplasm towards the insoluble nuclear matrix[15]. To detect an involvement of IQGAP1 in a similar regulation of hnRNPM's splicing activity through changes of its subnuclear distribution, we compared the localization of hnRNPM between parental and *IQGAP1*^{KO} cells, both untreated and after heat-shock (**Fig. 7a-b, 8c and Supplementary Fig. 7b**) using immunofluorescence and confocal microscopy. A clear difference in the subnuclear distribution of hnRNPM was detected between paternal and IQGAP1^{KO} cells, with the perinuclear enriched localization in parental cells changing to a more diffuse distribution, not only at the periphery of the nuclei, but also towards the inside of the nuclei (**Fig. 7a** and **Supplementary Fig. 7b**). As expected[15], hnRNPM's localization also changed from its perinuclear pattern to a granular one in the nucleus of parental cells upon heat-shock. Surprisingly, hnRNPM's localization and staining pattern did not further change upon heat-shock in cells lacking IQGAP1 (**Fig. 7a** and **Supplementary Fig. 7b**). The effect of heat shock on the alternative splicing of the DUP50 minigene reporter was also obvious in the parental cells, however such an effect was not apparent in cells lacking IQGAP1 (**Supplementary Fig. 7c**). To assay the localization of hnRNPM in relation to spliceosomal components, we compared it to that of SR proteins in untreated and heat-shocked parental and IQGAP1^{KO} cells (**Fig. 7b, c)**. Upon heat-shock, the colocalization between hnRNPM and SR proteins was reduced in the parental cells. hnRNPM and SR showed also decreased colocalization in untreated cells lacking IQGAP1, and no further change was induced upon heat-shock. Furthermore, the localization of SR proteins changes upon heat shock, and these changes seem to depend as well on the presence of

IQGAP1, suggesting a more general role of IQGAP1 for heat-shock response of the spliceosome machinery (**Fig. 7a-c**).

Since in heat-shocked cells hnRNPM moves away from spliceosomal components towards the nuclear matrix[15], we compared nuclear matrix preparations from parental and *IQGAP1*^{KO} cells before and after heat-shock. hnRNPM was detected elevated in the nuclear matrix of the parental cells after heat-shock compared to untreated cells, whereas this change was not detected in the *IQGAP1*^{KO} cells (**Fig. 8a**). Interestingly, IQGAP1 levels were also increased in nuclear matrix fractions prepared from heat-shocked cells (**Fig. 8a**). In agreement to this, increased nuclear IQGAP1 staining was detected in heat-shocked cells, compared to the untreated controls (**Supplementary Fig. 8a**). Using confocal microscopy and immunofluorescence staining, we compared the localization of hnRNPM to its interacting partner SFPQ (PSF) which is a known component of the nuclear matrix, interacting with the splicing machinery in soluble nucleoplasm[41]. The colocalization of hnRNPM and PSF was partial in untreated parental cells, and was significantly increased upon heat shock. Though, in untreated cells lacking IQGAP1, there was a higher percentage of colocalization between hnRNPM and SFPQ compared to parental cells, this was not affected upon heat shock (**Fig. 8b, c**).

Therefore, IQGAP1 is important for the proper subnuclear distribution of hnRNPM close to spliceosomal components (**Fig. 9)**. Upon heat-shock, hnRNPM translocates closer to nuclear matrix components and away from the spliceosomal components, only if IQGAP1 is present. Collectively, these results indicate the involvement of IQGAP1 in the response of alternative splicing regulating, nuclear ribonucleoproteins (RNPs) to stress, with a more significant role in regulating the splicing activity of hnRNPM-containing RNPs.

Discussion

Splicing regulatory networks are subject to signals modulating alternative exon choice. One of the best characterized AS changes in response to stress-signals is the shutdown of post-transcriptional pre-mRNA splicing observed in heat-shocked cells[42,16]. However, how this occurs mechanistically is still unknown. Here, we report the first insights for the roles of hnRNPM and IQGAP1 in mediating the response of alternative splicing factors to heat-induced stress. The fact that IQGAP1 is a scaffold protein with well-known roles in the cytoplasm as an integrator of many signalling cascades suggests that this may be a more general phenomenon. We show that in gastric cancer cells, the interaction of the two proteins, happens in fractions that are involved in post-transcriptional splicing and is necessary for the response of hnRNPM to heat-induced stress signals. Furthermore, we show here that nuclear IQGAP1 interacts with a large number of splicing regulators mostly in an RNA-dependent manner, in addition to its RNA-independent interaction with hnRNPM. Thus, based on our data, we propose that upon heat, and possibly other stressors, IQGAP1 and hnRNPM are removed from the spliceosome and move towards the less-well-defined nuclear matrix. IQGAP1 is not required for binding of hnRNPM to a reporter pre-mRNA *in vivo*, however, it is necessary for the function of hnRNPM, and possibly other factors in splicing, regulating the interaction of hnRNPM with spliceosomal components at distinct subnuclear compartments.

The nuclear translocation and localization of IQGAP1 appears to be cell-cycle dependent, since it is significantly increased in response to replication stress and subsequent G1/S arrest[27] and as presented herein, upon heat-shock. This finding complements prior reports suggesting IQGAP1 localization at the nuclear envelope during late mitotic stages[43]. Cyclebase data[44] suggest that hnRNPM is required for

progression of the cell cycle G1 phase. On the basis of our data, we propose that in the absence of IQGAP1, a number of pre-mRNAs involved in cell cycle regulation undergoes altered alternative splicing.

Specifically, IQGAP1 and hnRNPM seem to co-operatively regulate the AS of a cell-cycle RNA regulon. 5 out of the 10 cell division-related AS events that are deregulated in the absence of IQGAP1 are exon skipping events, characterized by the presence of the hnRNPM binding motif downstream of the alternative exon. Of these 5 events, ANAPC10 has the highest change in AS pattern upon IQGAP1 abrogation and a significant role in cell cycle regulation and cell division[34,35]. In cells with reduced amounts of both IQGAP1 and hnRNPM, ANAPC10 levels are reduced and at least a group of APC/C-CDH1 targets are specifically stabilized (TPX2, RRM2, TK1, CDH1 itself). Given the role of the controlled degradation of these proteins for cell cycle progression[35,45], we posit that these observations explain the aberrant cell cycle effect in the double KO cell lines, the multinucleated cells phenotype and the importance of the two proteins for gastric cancer development and progression as detected by the xenograft experiments.

Currently, the literature on alternative splicing, cell cycle control, multinucleated cancer cells and tumour growth is rather unclear and often conflicting. There is evidence connecting these cell cycle effects manifested as a balance between up-regulation or down-regulation of tumour growth[45–48]. Mitotic errors, such as mitotic exit defects can have distinct impacts at different points during tumour development[45]. Thus, targeting of the APC/C^{Cdh1} activity has been suggested as a possible tumour suppressive approach[34,45]. On the other hand, alternative splicing is subject to extensive periodic regulation during the cell cycle in a manner that is highly integrated with distinct layers of cell cycle control. Our data put these into context, leading to an experimentally

testable model in which IQGAP1 and hnRNPM co-operatively drive the balance towards tumour growth, and when they cannot interact, the balance is shifted towards tumour suppression. They accomplish this by adding a new level of control in the activity of the APC/C complex: alternative splicing regulation. If so, it is of critical importance to identify additional protein partners involved in this balancing mechanism, test its connection to specific cell-cycle stages and investigate whether this mechanism is involved both in additional cancer types and also in normal cells.

Methods

Cell culture. The human gastric cancer cell lines AGS, KATOIII, MKN45 and NUGC4 were a kind gift from P. Hatzis (B.S.R.C. "Al. Fleming", Greece). Cells were grown under standard tissue culture conditions (37^0C, 5% CO2) in RPMI medium (GIBCO), supplemented with 10% FBS, 1% sodium pyruvate and 1% penicillin–streptomycin. NUGC4 originated from a proximal metastasis in paragastric lymph nodes, and MKN45 was derived from liver metastasis. According to the GEMiCCL database, which incorporates data on cell lines from the Cancer Cell Line Encyclopedia, the Catalogue of Somatic Mutations in Cancer and NCI60[49], none of the gastric cancer cell lines tested have altered copy number of hnRNPM or IQGAP1. Only NUGC4 has a silent mutation c.2103G to A in *HNRNPM*, which is not included in the Single Nucleotide Variations (SNVs) or mutations referred by cBioportal in any cancer type[50,51].

Transfection of MKN45 and NUGC4 cells. Gastric cancer cell lines were transfected with plasmids pDUP51M1 or pDUP51-ΔM[31] (a gift from D. L. Black, UCLA, USA) and pCMS-EGFP (Takara Bio USA, Inc) or pEGFP-IQGAP1[52] [a gift from David

Sacks (Addgene plasmid # 30112; http://n2t.net/addgene:30112; RRID:Addgene_30112)], using the TurboFect transfection reagent (Thermo Fisher Scientific, Inc., MA). For RNA-mediated interference, cells were transfected with control siRNA (sc-37007, Santa Cruz Biotechnology, Inc., CA) or hnRNPM siRNA (sc-38286) at 30 nM final concentration, using the Lipofectamine RNAiMAX transfection reagent (Thermo Fisher Scientific), according to manufacturer's instructions.

Subcellular fractionation. The protocol for sub-cellular fractionation was as described before[30]. Briefly, for each experiment, approximately $1.0x10^7$-$1.0x10^8$ cells were harvested. The cell pellet was re-suspended in 3 to 5 volumes of hypotonic Buffer A (10 mM Tris-HCl, pH 7.4, 100 mM NaCl, 2.5 mM $MgCl_2$) supplemented with 0.5 % Triton X-100, protease and phosphatase inhibitors (1 mM NaF, 1 mM Na_3VO_4) and incubated on ice for 10 min. Cell membranes were sheared by passing the suspension 4-6 times through a 26-gauge syringe. Nuclei were isolated by centrifugation at 3000 x g for 10 min at 4°C, and the supernatant was kept as cytoplasmic extract. The nuclear pellet was washed once and the nuclei were resuspended in 2 volumes of Buffer A and sonicated twice for 5s (0.2A). Then, samples were centrifuged at 4000 x g for 10 min at 4°C. The upper phase, which is the nuclear extract, was collected, while the nuclear pellet was re-suspended in 2 volumes of 8 M Urea and stored at -20°C. Protein concentration of the isolated fractions was assessed using the Bradford assay[53].

For the subnuclear fractionation protocol that allows for analysis of the LASR complex[31] cells were harvested, incubated on ice in Buffer B (10 mM HEPES-KOH pH 7.5, 15 mM KCl, 1.5 mM EDTA, 0.15 mM spermine) for 30 min and lysed with the addition of 0.3 % Triton X-100. Nuclei were collected by centrifugation and further purified by re-suspending the pellet in S1 buffer (0.25M Sucrose, 10 mM $MgCl_2$) and

laid over an equal volume of S2 buffer (0.35 M Sucrose, 0.5 mM $MgCl_2$). Purified nuclei were lysed in ten volumes of ice-cold lysis buffer (20 mM HEPES-KOH pH 7.5, 150 mM NaCl, 1.5 mM $MgCl_2$, 0.5 mM DTT and 0.6 % Triton X-100) and nucleosol was separated via centrifugation from the high molecular weight fraction (pellet). The high molecular weight (HMW) fraction was subsequently resuspended in Buffer B and treated with either DNase I (0.1 mg/ml) or RNase A (0.1 mg/ml). The supernatant was collected by centrifugation at 20,000 x g for 5 min, as the HMW treated sample.

The nuclear matrix fractionation was as previously described[54]. Briefly, cells were harvested and washed with PBS. The cell pellet obtained was re-suspended in a five packed cell pellet volumes of buffer A (10 mM Tris-HCl pH 7.5, 2.5 mM $MgCl_2$, 100 mM NaCl, 0.5% Triton X-100, 0.5 mM DTT and protease inhibitors) and incubated on ice for 15 min. The cells were then collected by centrifugation at 2000rpm for 10 min and re-suspended in 2 volumes of buffer A. To break the plasma membrane a Dounce homogenizer (10 strokes) was used and the cells were checked under the microscope. After centrifugation at 2000 rpm for 5 min, supernatant was gently removed and kept as cytoplasmic fraction, while the pellet containing the nuclei was re-suspended in 10 packed nuclear pellet volumes of S1 solution (0.25 M sucrose, 10 mM $MgCl_2$), on top of which an equal volume of S2 solution (0.35 M sucrose, 0.5 mM $MgCl_2$) was layered. After centrifugation at 2800 x g for 5 min, the nuclear pellet was re-suspended in 10 volumes of buffer NM (20 mM HEPES pH 7.4, 150 mM NaCl, 2.5 mM $MgCl_2$, 0.6 % Triton X-100 and Protease inhibitors) and lysed on ice for 10 minutes, followed by centrifugation as above. The supernatant was removed and kept as nuclear extract while the pellet was re-suspended in buffer A containing DNase I (0.5mg/mL) or RNase A (0.1 mg/mL) and Protease inhibitors and stirred gently at room temperature for 30

minutes. The upper phase defining the nuclear matrix fraction was quantified and stored at -20˚C.

Immunoprecipitation. Co-immunoprecipitation of proteins was performed using Protein A/G agarose beads (Protein A/G Plus Agarose Beads, Santa-Cruz Biotechnologies, sc-2003) as follows: 20 µl of bead slurry per immunoprecipitation reaction was washed with NET-2 buffer (10 mM Tris pH 7.5, 150 mM NaCl, 0.05 % NP-40). 4-8 µg of antibody were added to a final volume of 500-600 µL in NET-2 buffer per sample. Antibody binding was performed by overnight incubation at 4ºC on a rotating wheel. Following the binding of the antibody, beads were washed at least 3 times by resuspension in NET-2. For each IP sample, 500-1000 µg of protein were added to the beads, in a final volume of 800 µL with NET-2 buffer and incubated for 2 hrs at 4ºC on a rotating wheel. After sample binding, beads were washed 3 times with NET-2 buffer, and twice with NET-2 buffer supplemented with 0.1% Triton X-100 and a final concentration of 0.1% NP-40. For the UV-crosslinking experiments, beads were washed five times with wash buffer containing 1M NaCl and twice with standard wash buffer. Co-immunoprecipitated proteins were eluted from the beads by adding 15-20 µL of 2x Laemmli sample buffer (0.1 M Tris, 0.012% bromophenol blue, 4 % SDS, 0.95 M β-mercapthoethanol, 12 % glycerol) and boiled at 95ºC for 5 min. Following centrifugation at 10.000 x g for 2 min, the supernatant was retained and stored at -20ºC or immediately used.

Western Blot analysis. Cell lysate (7-10 µg for nuclear lysates and 15-20 µg for the cytoplasmic fraction) was resolved on an 8%, 10% or 12 % SDS-polyacrylamide gel and transferred to a polyvinylidinedifluoride membrane (PVDF, Millipore). Primary antibodies were added and the membranes were incubated overnight at 4˚C. Antibodies were used against: hnRNPM (1:500, clone 1D8, sc-20002), IQGAP1 (1:1000, clone

H109, sc-10792; 1:1000, clone C-9, sc-379021; 1:1000 clone D-3, sc-374307, all from Santa Cruz), beta-actin (1:1000, clone 7D2C10, 60008-1-Ig, ProteinTech), Lamin B1 (1:1000, clone A-11, sc-377000, Santa Cruz), GAPDH (1:2000, 60004-1-Ig, ProteinTech), hnRNP A2/B1 (1:1000, clone DP3B3, sc-32316, Santa Cruz), SRSF1 (SF2/ASF; 1:1000, SC-33652, Santa Cruz), hnRNP A1 (1:1000, clone 4B10, sc-32301, Santa Cruz), hnRNPL (1:1000, clone 4D11, sc-32317, Santa Cruz), hnRNP C1/C2 (1:1000, clone 4F4, sc-32308, Santa Cruz), DHX9/RHA (1:1000, ab26271, Abcam), hnRNP K/J (1:1000, clone 3C2, sc-32307, Santa Cruz), SF3B3 (1:1000, clone B-4, sc-398670, Santa-Cruz), beta tubulin (1:1000, clone 2-28-33, Sigma-Aldrich), TPX2 (1:200, clone E-2, sc-271570, Santa Cruz), RRM2 (1:200, clone A-5, sc-398294, Santa Cruz), SAFB (1:1000, F-3, sc-393403, Santa Cruz), Matrin3 (1:1000, 2539C3a, Santa Cruz), Histone-H3 (1:2000, 17168-AP, ProteinTech), DDX17 (clone H-7, sc-398168, Santa Cruz), CPSF6 (1:1000, sc-292170, Santa Cruz), NF90 (1:1500, clone A-3, sc-377406, Santa Cruz), anillin (1:1000, CL0303, ab211872, Abcam) , FZR (1:200, clone DCS-266, sc-56312, Santa Cruz), TK1 (1:5000, clone EPR3193, ab76495, Abcam), ANAPC10 (1:100, clone B-1, sc-166790, Santa Cruz). HRP-conjugated goat anti-mouse IgG (1:5000, 1030-05, SouthernBiotech) or HRP-conjugated goat anti-rabbit IgG (1:5000, 4050-05, SouthernBiotech) were used as secondary antibodies. Detection was carried out using Immobilon Crescendo Western HRP substrate (WBLUR00500, Millipore).

Generation of knockouts. The CRISPR/Cas9 strategy was used to generate IQGAP1 knockout cells[55]. Exon1 of the *IQGAP1* transcript was targeted using the following pair of synthetic guide RNA (sgRNA) sequences: Assembly 1: 5'-CACTATGGCTGTGAGTGCG-3' and Assembly 2: 5'-CAGCCCGTCAACCTCGTCTG-3'. The sequences were identified using the CRISPR

Design tool (http://crispr.mit.edu/). These sequences and their reverse complements were annealed and ligated into the BbSI and BsaI sites of the All-In-One vector [AIO-Puro, a gift from Steve Jackson (Addgene plasmid #74630; http://n2t.net/addgene:74630; RRID:Addgene_74630)][56]. The two pairs of complementary DNA-oligos (Assemblies 1 and 2 including a 4-mer overhang + 20-mer of sgRNA sequence) were purchased from Integrated DNA technologies (IDT). The insertion of sgRNAs was verified via sequencing. MKN45 and NUGC4 cells were transfected using Lipofectamine 2000, and clones were selected 48 h later using puromycin. Individual clones were plated to single cell dilution in 24 well-plates, and IQGAP1 deletion was confirmed by PCR of genomic DNA using the following primers: Forward: 5'-GCCGTCCGCGCCTCCAAG-3'; Reverse: 5'-GTCCGAGCTGCCGGCAGC-3' and sequencing using the Forward primer. Loss of IQGAP1 protein expression was confirmed by Western Blotting. MKN45 and NUGC4 cells transfected with AIO-Puro empty vector were selected with puromycin and used as a control during the clone screening process.

For the generation of the *hnRNPM* ^{KO} cells we used a different approach. We ordered a synthetic guide RNA (sgRNA) (5'- CGGCGTGCCGAGCGGCAACG-3'), targeting exon 1 of the *hnRNPM* transcript, in the form of crRNA from IDT, together with tracrRNA. We assembled the tracrRNA:crRNA duplex by combining 24pmol of tracRNA and 24pmol of crRNA in a volume of 5µl, and incubating at 95°C for 5 min, followed by incubation at room temperature. 12pmol of recombinant Cas9 (Protein Expression and Purification Facility, EMBL, Heidelberg) were mixed with 12pmol of the tracrRNA:crRNA duplex in OPTIMEM I (GIBCO) for 5min at room temperature and this RNP was used to transfect MKN45 cells in the presence of Lipofectamine RNAiMax. Cells were harvested 48 h later and individual clones were isolated and

assayed for hnRNPM downregulation as described above for IQGAP1. The primers used were: Forward: 5'- CACGTGGGCGCGCAGG -3'; Reverse: 5'-GCAAAGGACCGTGGGATACTCAC -3.

Splicing assay. Splicing assays with the DUP51M1 and DUP50M1 mini-gene reporters were performed as previously described[31]. Briefly, cells were co-transfected with DUP51M1 (or DUP50M1) or DUP51-ΔM (or DUP50-ΔM) site plasmids and pCMS-EGFP at 1:3 ratio for 40 h. Total RNA was extracted using TRIzol Reagent® (Thermo Fisher Scientific) and cDNA was synthesized in the presence of a DUP51-specific primer (DUP51-RT, 5'-AACAGCATCAGGAGTGGACAGATCCC-3'). Analysis of alternative spliced transcripts was carried out with PCR (15-25 cycles) using primers DUP51S_F (5'-GACACCATCCAAGGTGCAC-3') and DUP51S_R (5'-CTCAAAGAACCTCTGGGTCCAAG-3'), followed by electrophoresis on 8% acrylamide-urea gel. Quantification of percentage of exon 2 inclusion was performed with ImageJ or with ImageLab software (version 5.2, Bio-Rad Laboratories) when ^{32}P-labelled DUP51S_F primer was used for the PCR. For the detection of the RNA transcript bound on hnRNPM after UV crosslinking, PCR was performed using primers DUP51UNS_F (5'-TTGGGTTTCTGATAGGCACTG-3') and DUP51S_R (see above).

For the validation of the AS events identified by RNA-seq, cDNA was synthesized from total RNA of appropriate cells in the presence of random hexamer primers and used as a template in PCR with the primers listed in **Supplementary Table 4**. % inclusion for each event in 3 or more biological replicates was analysed in 8% acrylamide-urea gel and quantified by ImageJ.

UV-crosslinking experiments were performed as described[31]. Briefly, monolayer MKN45 cell cultures after transfection with the minigene reporters, as described above,

were irradiated with UV (254 nm) at 75 mJ/cm^2 on ice in a UV irradiation system BLX 254 (Vilber Lourmat). UV-irradiated cells were lysed for 5 min on ice with ten packed cell volumes of buffer [20 mM HEPES-KOH pH 7.5, 150 mM NaCl, 0.5 mM DTT, 1 mM EDTA, 0.6% Triton X-100, 0.1% SDS, and 50mg/ml yeast tRNA] and centrifuged at 20,000 x g for 5 min at 4^{0}C. The supernatants were 5 x diluted with buffer [20 mM HEPES-KOH pH 7.5, 150 mM NaCl, 0.5 mM DTT, 1 mM EDTA, 1.25x Complete protease inhibitors (Roche), and 50 μg/ml yeast tRNA]. Lysates were centrifuged for 10 min at 20,000 x g, 4^{0}C prior to IP.

MTT cell proliferation assay. In 96-well plates, cells were seeded at a density of 2×10^3 cells/well in complete RPMI. After 24 hrs, the medium was replaced with serum-free RPMI supplemented with 0.5mg/ml MTT (3-[4,5-dimethylthiazol-2-yl]-2,5-diphenyl tetrazolium bromide; Sigma-Aldrich) colorimetric staining solution for 2h. After the removal of MTT, the cells were mixed with 200μl DMSO and incubated for 5-10min at RT on a shaking platform. The absorbance was read at 570 nm using the SUNRISE™ Absorbance Reader (Tecan Trading AG).

Colony-Formation assay. In 6-well plates, 200 cells/well were placed and allowed to grow for 7 days at 37°C with 5% CO_2. The formed colonies were fixed with 0.5mL of 100% methanol for 20min at RT. Methanol was then removed and cells were carefully rinsed with H_2O. 0.5ml crystal violet staining solution (0.5% crystal violet in 10% ethanol) was added to each well and cells were left for 5min at RT. The plates were then washed with H_2O until excess dye was removed and were left to dry. The images were captured by Molecular Imager® ChemiDoc™ XRS+ Gel Imaging System (Bio-Rad) and colonies were quantified using ImageJ software.

Wound healing assay. Cells were cultured in 24-well plates at 37°C with 5% CO_2 in a monolayer, until nearly 90% confluent. Scratches were then made with a sterile 200μl

pipette tip and fresh medium without FBS was gently added. The migration of cells in the same wound area was visualized at 0, 8, 24, 32 and 48 hrs using Axio Observer A1 (Zeiss) microscope with automated stage.

Cell Cycle Analysis. The cells were seeded in 6-well plates at a density of 3×10^5 cells/well. When cells reached 60-80% confluence, they were harvested by trypsinization into phosphate-buffered saline (PBS). The pellets were fixed in 70% ethanol and stored at -20°C till all time-points were collected. On the day of the FACS analysis, cell pellets were washed in phosphate-citrate buffer and centrifuged for 20min. 250μl of RNase/propidium iodide (PI) solution were then added to each sample (at concentrations of 100μg/ml for RNase and 50μg/ml for PI) and cells were incubated at 37°C for 30min. Finally, the cells were analysed through flow cytometric analysis using FACSCanto^{TM} II (BD-Biosciences).

Mouse Xenograft study. Experiments were performed in the animal facilities of Biomedical Sciences Research Center (BSRC) "Alexander Fleming" and were approved by the Institutional Committee of Protocol Evaluation in conjunction with the Veterinary Service Management of the Hellenic Republic Prefecture of Attika according to all current European and national legislation and performed in accordance with the guidance of the Institutional Animal Care and Use Committee of BSRC "Alexander Fleming". 1 x10^6 cells of MKN45, MKN45-IQGAP1^{KO}, MKN45-hnRNP-M^{KO} or double KO cells were injected into the flank of 8-10-week-old NOD-SCID[57] both male and female mice randomly distributed among groups. Groups of 11 mice were used per cell type, based on power analysis performed using the following calculator: https://www.stat.ubc.ca/~rollin/stats/ssize/n2.html. Tumour growth was monitored up to 4 weeks and recorded by measuring two perpendicular diameters using the formula 1/2(Length × Width^2) bi-weekly[58]. During the experiment, the investigator

contacting the measurements was unaware of the sample group allocation (blinded experiment). At end-point, mice were euthanized and tumours were collected and enclosed in paraffin for further analyses.

Immunostaining. For immunofluorescence, cells were seeded on glass coverslips and were left to adhere for 24 hrs. Cells were next fixed for 10 minutes with 4% paraformaldehyde PFA (Alfa Aesar), followed by permeabilization with 0.25% (w/v) Triton X-100. Cells were then incubated for 30 min in 5% BSA/PBS (phosphate buffer saline). The primary antibodies used for immunostaining were: anti-hnRNPM (1:300, clone 1D8, NB200-314SS, Novus or 1:100, NBP1-84555, Novus), anti-IQGAP1 (1:500, ab86064, Abcam or 1:250 sc-374307, Santa-Cruz), anti-SR (1:100, clone 1H4, sc-13509, Santa-Cruz), recognizing SRp75, SRp55, SRp40, SRp30a/b and SRp20, anti-PSF (1:100, clone H-80, sc-28730, Santa-Cruz). For β-TUBULIN staining, cells were fixed in -20°C with ice-cold methanol for 3 minutes, blocked in 1% BSA/PBS solution and incubated overnight with the primary antibody (1:250, clone 2-28-33, Sigma-Aldrich). After washing with PBS, cells were incubated with secondary antibodies (anti-rabbit-Alexa Fluor 555 or anti-mouse Alexa Fluor 488, both used at 1:500; Molecular Probes) at room temperature for 1h followed by the staining of nuclei with DAPI for 5 min at RT. For mounting Mowiol mounting medium (Sigma-Aldrich) was used and the images were acquired with Leica DM2000 fluorescence microscope or a LEICA SP8 White Light Laser confocal system and were analysed using the Image J software.

Tissue Microarrays (TMA) slides were purchased from US Biomax, Inc (cat. no. T012a). The slides were deparaffinized in xylene and hydrated in different alcohol concentrations. Heat-induced antigen retrieval in citrate buffer pH 6.0 was used.

Blocking, incubation with first and secondary antibodies as well as the nuclei staining and mounting, were performed as mentioned above.

Microscopy and image analysis. Fluorescent images were acquired with a Leica TCS SP8 X confocal system equipped with an argon and a supercontinuum white light laser source, using the LAS AF software (Leica). The same acquisition settings were applied for all samples. Pixel-based colocalization analysis was performed with the Image J software, using the "Colocalization Threshold" plugin[59] (Costes et al, 2002) to calculate the Pearson correlation coefficient. Image background was subtracted using the "Substract background" function of Image J (50px ball radius). For each image, the middle slices representing the cell nuclei (selected as regions of interest (ROI) based on the DAPI signal) were chosen for analysis and at least 30 cells or more were analysed for each cell line. Intensity plot profiles (k-plots) were generated using the "Plot profile" function of Image J. After background substraction (as mentioned above), a line was drawn across each cell and the pixel gray values for hnRNPM, SR & PSF signals were acquired. Adobe Photoshop CS6 was used for merging the final images, where brightness and contrast were globally adjusted.

Immunohistochemistry and H&E staining. At the end of the xenograft experiment tumours were dissected from the mice, fixed in formalin and embedded in paraffin. Sections were cut at 5 μm thickness, were de-paraffinized and stained for haematoxylin and eosin. For IHC, after de-paraffinization serial sections were hydrated, incubated in 3% H_2O_2 solution for 10 minutes, washed and boiled at 95°C for 15 minutes in sodium citrate buffer pH 6.0 for antigen retrieval. Blocking was performed with 5% BSA for 1 hr and sections were then incubated with the following primary antibodies overnight at 4°C diluted in BSA: anti Ki-67 (1:200, clone 14-5698-82, ThermoFisher Scientific), hnRNP-M (1:100, clone 1D8, sc-20002, Santa Cruz), IQGAP1 (1:100, ab86064,

Abcam). Sections were subsequently washed and incubated with the appropriate secondary antibody conjugated to HRP, HRP-conjugated goat anti-mouse IgG (1:5000, 1030-05, SouthernBiotech) or HRP-conjugated goat anti-rabbit IgG (1:5000, 4050-05, SouthernBiotech) and the DAB Substrate Kit (SK-4100, Vector Laboratories) was used to visualise the signal. The sections were counterstained with hematoxylin and imaged with a NIKON Eclipse E600 microscope, equipped with a Qcapture camera.

Proximity ligation assay. Cells were grown on coverslips (13 mM diameter, VWR) and fixed for 10 min with 4% PFA (Alfa Aesar), followed by 10 min permeabilization with 0.25% Triton X-100 in PBS and blocking with 5% BSA in PBS for 30 min. Primary antibodies: anti-hnRNPM (1:300, clone 1D8, NB200-314SS, Novus), anti-IQGAP1 (1:500, ab86064, Abcam or 1:500, 22167-1-AP, Proteintech) diluted in blocking buffer were added and incubated overnight at 4˚C. Proximity ligation assays were performed using the Duolink kit (Sigma-Aldrich DUO92102), according to manufacturer's protocol. Images were collected using a Leica SP8 confocal microscope.

RNA isolation and reverse transcription. Total RNA was extracted with the TRIzol® reagent (Thermo Fisher Scientific). DNA was removed with RQ1 RNase-free DNase (Promega, WI) or DNase I (RNase-free, New England Biolabs, Inc, MA), followed by phenol extraction. Reverse transcription was carried with 0.4-1 μg total RNA in the presence of gene-specific or random hexamer primers, RNaseOUT™ Recombinant Ribonuclease Inhibitor (Thermo Fisher Scientific) and SuperScript® III (Thermo Fisher Scientific) or Protoscript II (New England Biolabs) reverse transcriptase, according to manufacturer's instructions.

Mass spectrometry and Proteomics analysis. Anti-IQGAP1 immunoprecipitation samples were processed in collaboration with the Core Proteomics Facility at EMBL Heidelberg. Proteomics analysis[60] was performed as follows: samples were dissolved in 2x Laemmli sample buffer, and underwent filter-assisted sample preparation (FASP) to produce peptides with proteolytic digestion[61]. These were then tagged using 4 different multiplex TMT isobaric tags (ThermoFisher Scientific, TMTsixplex™ Isobaric Label Reagent Set): one isotopically unique tag for each IP condition, namely IQGAP1 IP cancer (NUGC4) and the respective IgG control. TMT-tagged samples were appropriately pooled and analysed using HPLC-MS/MS. Three biological replicates for each IP condition were processed.

Samples were processed using the ISOBARQuant[62], an R-package platform for the analysis of isobarically labelled quantitative proteomics data. Only proteins that were quantified with two unique peptide matches were filtered. After batch-cleaning and normalization of raw signal intensities, fold-change was calculated. Statistical analysis of results was performed using the LIMMA[63] R-package, making comparisons between each IQGAP1 IP sample and their respective IgG controls. A protein was considered significant if it had a *P*value < 5% (Benjamini-Hochberg FDR adjustment), and a fold-change of at least 50% between compared conditions. Identified proteins were classified into 3 categories: Hits (FDR threshold= 0.05, fold change=2), candidates (FDR threshold = 0.25, fold change = 1.5), and no hits (see **Supplementary Table 1**). For the differential proteome analysis of MKN45 and MKN45-*IQGAP1*^{KO} cells, whole cell lysates were prepared in RIPA buffer [25 mM Tris-HCl (pH 7.5), 150 mM NaCl, 1% NP-40, 0.5% sodium deoxycholate, 0.1% SDS). Samples underwent filter-assisted sample preparation (FASP) to produce peptides with proteolytic digestion[61] and

analysed using HPLC-MS/MS. The full dataset is being prepared to be published elsewhere.

RNA-seq analysis. Total TRIzol-extracted RNA was treated with RQ1-RNase free DNase (Promega). cDNA libraries were prepared in collaboration with Genecore, at EMBL, Heidelberg. Alternative splicing was analyzed by using VAST-TOOLS v2.2.2[64] and expressed as changes in percent-spliced-in values (ΔPSI). A minimum read coverage of 10 junction reads per sample was required, as described[64]. Psi values for single replicates were quantified for all types of alternative events. Events showing splicing change (|ΔPSI|> 15 with minimum range of 5% between control and *IQGAP1*^{KO} samples were considered IQGAP1-regulated events.

ORF impact prediction. Potential ORF impact of alternative exons was predicted as described[64]. Exons were mapped on the coding sequence (CDS) or 5'/3' untranslated regions (UTR) of genes. Events mapping on the CDS were divided in CDS-preserving or CDS-disrupting.

RNA maps. We compared sequence of introns surrounding exons showing more inclusion or skipping in IQGAP1^{KO} samples with a set of 1,050 not changing alternative exons. To generate the RNA maps, we used the rna_maps function[65], using sliding windows of 15 nucleotides. Searches were restricted to the affected exons, the first and last 500 nucleotides of the upstream and downstream intron and 50 nucleotides into the upstream and downstream exons. Regular expression was used to search for the binding motif of hnRNPM (GTGGTGG|GGTTGGTT|GTGTTGT|TGTTGGAG or GTGGTGG|GGTTGGTT|TGGTGG|GGTGG)[13].

Gene Ontology. Enrichment for GO terms was analyzed using ShinyGO v0.61[66] with *P* value cut-off (FDR) set at 0.05.

Data availability

The mass spectrometry proteomics data have been deposited to the ProteomeXchange Consortium via the PRIDE68 partner repository[67] with the dataset identifier PXD017842.

RNA-seq data have been deposited in GEO: GSE146283.

Furthermore, the data and/or reagents that support the findings of this study are available from the corresponding author, P.K., upon reasonable request.

Source data for Figs. 1-7 and Supplementary Data Figs. 1-6 will be provided online.

References

1. Wang, Z. & Burge, C. B. Splicing regulation: From a parts list of regulatory elements to an integrated splicing code. RNA 14, 802–813 (2008).

2. Pan, Q., Shai, O., Lee, L. J., Frey, B. J. & Blencowe, B. J. Deep surveying of alternative splicing complexity in the human transcriptome by high-throughput sequencing. Nat. Genet. 40, 1413–1415 (2008).

3. Heyd, F. & Lynch, K. W. Degrade, move, regroup: signaling control of splicing proteins. Trends Biochem. Sci. 36, 397–404 (2011).

4. El Marabti, E. & Younis, I. The Cancer Spliceome: Reprograming of Alternative Splicing in Cancer. Front. Mol. Biosci. 5, (2018).

5. Oltean, S. & Bates, D. O. Hallmarks of alternative splicing in cancer. Oncogene (2013) doi:10.1038/onc.2013.533.

6. Sveen, A., Kilpinen, S., Ruusulehto, A., Lothe, R. A. & Skotheim, R. I. Aberrant RNA splicing in cancer; expression changes and driver mutations of splicing factor genes. Oncogene (2015) doi:10.1038/onc.2015.318.

7. Kahles, A. et al. Comprehensive Analysis of Alternative Splicing Across Tumours from 8,705 Patients. Cancer Cell 34, 211-224.e6 (2018).

8. Shkreta, L. & Chabot, B. The RNA Splicing Response to DNA Damage. Biomolecules 5, 2935–2977 (2015).

9. Datar, K. V., Dreyfuss, G. & Swanson, M. S. The human hnRNP M proteins: identification of a methionine/arginine-rich repeat motif in ribonucleoproteins. Nucleic Acids Res. 21, 439–446 (1993).

10. Kafasla, P., Patrinou-Georgoula, M., Lewis, J. D. & Guialis, A. Association of the 72/74-kDa proteins, members of the heterogeneous nuclear ribonucleoprotein M group, with the pre-mRNA at early stages of spliceosome assembly. Biochem. J. 363, 793–799 (2002).

11. Llères, D., Denegri, M., Biggiogera, M., Ajuh, P. & Lamond, A. I. Direct interaction between hnRNP-M and CDC5L/PLRG1 proteins affects alternative splice site choice. EMBO Rep. 11, 445–451 (2010).

12. Hovhannisyan, R. H. & Carstens, R. P. Heterogeneous ribonucleoprotein m is a splicing regulatory protein that can enhance or silence splicing of alternatively spliced exons. J. Biol. Chem. 282, 36265–36274 (2007).

13. Huelga, S. C. et al. Integrative Genome-wide Analysis Reveals Cooperative Regulation of Alternative Splicing by hnRNP Proteins. Cell Rep. 1, 167–178 (2012).

14. Pervouchine, D. et al. Integrative transcriptomic analysis suggests new autoregulatory splicing events coupled with nonsense-mediated mRNA decay. Nucleic Acids Res. 47, 5293–5306 (2019).

15. Gattoni, R. et al. The human hnRNP-M proteins: structure and relation with early heat shock-induced splicing arrest and chromosome mapping. Nucleic Acids Res. 24, 2535–2542 (1996).

16. Shalgi, R., Hurt, J. A., Lindquist, S. & Burge, C. B. Widespread Inhibition of Posttranscriptional Splicing Shapes the Cellular Transcriptome following Heat Shock. *Cell Reports* **7**, 1362–1370 (2014).

17. Xu, Y. et al. Cell type-restricted activity of hnRNPM promotes breast cancer metastasis via regulating alternative splicing. Genes Dev. 28, 1191–1203 (2014).

18. Harvey, S. E. et al. Coregulation of alternative splicing by hnRNPM and ESRP1 during EMT. RNA 24, 1326–1338 (2018).

19. Hu, X. et al. The RNA-binding protein AKAP8 suppresses tumour metastasis by antagonizing EMT-associated alternative splicing. Nat. Commun. 11, 486 (2020).

20. Passacantilli, I., Frisone, P., De Paola, E., Fidaleo, M. & Paronetto, M. P. hnRNPM guides an alternative splicing program in response to inhibition of the PI3K/AKT/mTOR pathway in Ewing sarcoma cells. Nucleic Acids Res. 45, 12270–12284 (2017).

21. West, K. O. et al. The Splicing Factor hnRNP M Is a Critical Regulator of Innate Immune Gene Expression in Macrophages. Cell Rep. 29, 1594-1609.e5 (2019).

22. Smith, J. M., Hedman, A. C. & Sacks, D. B. IQGAPs choreograph cellular signaling from the membrane to the nucleus. Trends Cell Biol. 25, 171–184 (2015).

23. Osman, M. A., Sarkar, F. H. & Rodriguez-Boulan, E. A molecular rheostat at the interface of cancer and diabetes. Biochim. Biophys. Acta 1836, 166–176 (2013).

24. White, C. D., Brown, M. D. & Sacks, D. B. IQGAPs in cancer: A family of scaffold proteins underlying tumourigenesis. FEBS Lett. 583, 1817–1824 (2009).

25. Hu, W. et al. IQGAP1 promotes pancreatic cancer progression and epithelial-mesenchymal transition (EMT) through Wnt/β-catenin signaling. Sci. Rep. 9, 7539 (2019).

26. Li, S., Wang, Q., Chakladar, A., Bronson, R. T. & Bernards, A. Gastric Hyperplasia in Mice Lacking the Putative Cdc42 Effector IQGAP1. Mol. Cell. Biol. 20, 697–701 (2000).

27. Johnson, M., Sharma, M., Brocardo, M. G. & Henderson, B. R. IQGAP1 translocates to the nucleus in early S-phase and contributes to cell cycle progression after DNA replication arrest. Int. J. Biochem. Cell Biol. 43, 65–73 (2011).

28. Cvitkovic, I. & Jurica, M. S. Spliceosome database: a tool for tracking components of the spliceosome. Nucleic Acids Res. 41, D132-141 (2013).

29. Choi, Y. D. & Dreyfuss, G. Isolation of the heterogeneous nuclear RNA-ribonucleoprotein complex (hnRNP): a unique supramolecular assembly. Proc. Natl. Acad. Sci. U. S. A. 81, 7471–7475 (1984).

30. Kafasla, P., Patrinou-Georgoula, M. & Guialis, A. The 72/74-kDa polypeptides of the 70-110 S large heterogeneous nuclear ribonucleoprotein complex (LH-nRNP) represent a discrete subset of the hnRNP M protein family. Biochem. J. 350 Pt 2, 495–503 (2000).

31. Damianov, A. et al. Rbfox Proteins Regulate Splicing as Part of a Large Multiprotein Complex LASR. Cell 165, 606–619 (2016).

32. Zhu, Y. et al. POSTAR2: deciphering the post-transcriptional regulatory logics. Nucleic Acids Res. 47, D203–D211 (2019).

33. Van Nostrand, E. L. et al. Robust transcriptome-wide discovery of RNA-binding protein binding sites with enhanced CLIP (eCLIP). Nat. Methods 13, 508–514 (2016).

34. Yamano, H. APC/C: current understanding and future perspectives. F1000Research 8, (2019).

35. Zhou, Z., He, M., Shah, A. A. & Wan, Y. Insights into APC/C: from cellular function to diseases and therapeutics. Cell Div. 11, 9 (2016).

36. da Fonseca, P. C. A. et al. Structures of APC/C(Cdh1) with substrates identify Cdh1 and Apc10 as the D-box co-receptor. Nature 470, 274–278 (2011).

37. Alfieri, C., Zhang, S. & Barford, D. Visualizing the complex functions and mechanisms of the anaphase promoting complex/cyclosome (APC/C). Open Biol. 7, (2017).

38. Engström, Y. et al. Cell cycle-dependent expression of mammalian ribonucleotide reductase. Differential regulation of the two subunits. J. Biol. Chem. 260, 9114–9116 (1985).

39. Neumayer, G., Belzil, C., Gruss, O. J. & Nguyen, M. D. TPX2: of spindle assembly, DNA damage response, and cancer. Cell. Mol. Life Sci. CMLS 71, 3027–3047 (2014).

40. Sherley, J. L. & Kelly, T. J. Regulation of human thymidine kinase during the cell cycle. J. Biol. Chem. 263, 8350–8358 (1988).

41. Meissner, M. *et al.* Differential nuclear localization and nuclear matrix association of the splicing factors PSF and PTB. *J. Cell. Biochem.* **76**, 559–566 (2000).

42. Biamonti, G. & Caceres, J. F. Cellular stress and RNA splicing. Trends Biochem. Sci. 34, 146–153 (2009).

43. Lian, A. T., Hains, P. G., Sarcevic, B., Robinson, P. J. & Chircop, M. IQGAP1 is associated with nuclear envelope reformation and completion of abscission. Cell Cycle 14, 2058–2074 (2015).

44. Cyclebase 3.0: a multi-organism database on cell-cycle regulation and phenotypes | Nucleic Acids Research | Oxford Academic. https://academic.oup.com/nar/article/43/D1/D1140/2437426.

45. Penas, C., Ramachandran, V. & Ayad, N. G. The APC/C Ubiquitin Ligase: From Cell Biology to Tumourigenesis. Front. Oncol. 1, 60 (2011).

46. Levine, M. S. & Holland, A. J. The impact of mitotic errors on cell proliferation and tumourigenesis. Genes Dev. 32, 620–638 (2018).

47. Sansregret, L. et al. APC/C Dysfunction Limits Excessive Cancer Chromosomal Instability. Cancer Discov. 7, 218–233 (2017).

48. Gijn, S. E. van et al. TPX2/Aurora kinase A signaling as a potential therapeutic target in genomically unstable cancer cells. Oncogene 38, 852–867 (2019).

49. Jeong, I. et al. GEMiCCL: mining genotype and expression data of cancer cell lines with elaborate visualization. Database 2018, (2018).

50. Gao, J. et al. Integrative analysis of complex cancer genomics and clinical profiles using the cBioPortal. Sci. Signal. 6, pl1 (2013).

51. Cerami, E. et al. The cBio cancer genomics portal: an open platform for exploring multidimensional cancer genomics data. Cancer Discov. 2, 401–404 (2012).

52. Ren, J.-G., Li, Z., Crimmins, D. L. & Sacks, D. B. Self-association of IQGAP1: characterization and functional sequelae. J. Biol. Chem. 280, 34548–34557 (2005).

53. Bradford, M. M. A rapid and sensitive method for the quantification of microgram quantities of protein utilizing the principle of protein-dye binding. Anal. Biochem. 72, 248–254 (1976).

54. Mähl, P., Lutz, Y., Puvion, E. & Fuchs, J. P. Rapid effect of heat shock on two heterogeneous nuclear ribonucleoprotein-associated antigens in HeLa cells. J. Cell Biol. 109, 1921–1935 (1989).

55. Ran, F. A. et al. Genome engineering using the CRISPR-Cas9 system. Nat. Protoc. 8, 2281–2308 (2013).

56. Chiang, T.-W. W., le Sage, C., Larrieu, D., Demir, M. & Jackson, S. P. CRISPR-Cas9D10A nickase-based genotypic and phenotypic screening to enhance genome editing. Sci. Rep. 6, 24356 (2016).

57. Shultz, L. D. et al. Multiple defects in innate and adaptive immunologic function in NOD/LtSz-scid mice. J. Immunol. Baltim. Md 1950 154, 180–191 (1995).

58. Euhus, D. M., Hudd, C., LaRegina, M. C. & Johnson, F. E. Tumour measurement in the nude mouse. J. Surg. Oncol. 31, 229–234 (1986).

59. Costes, S. V. *et al.* Automatic and Quantitative Measurement of Protein-Protein Colocalization in Live Cells. *Biophysical Journal* **86**, 3993–4003 (2004).

60. Aebersold, R. & Mann, M. Mass spectrometry-based proteomics. Nature 422, 198–207 (2003).

61. Wiśniewski, J. R., Zougman, A., Nagaraj, N. & Mann, M. Universal sample preparation method for proteome analysis. Nat. Methods 6, 359–362 (2009).

62. Breitwieser, F. P. et al. General Statistical Modeling of Data from Protein Relative Expression Isobaric Tags. J. Proteome Res. 10, 2758–2766 (2011).

63. Smyth, G. K. Linear models and empirical bayes methods for assessing differential expression in microarray experiments. Stat. Appl. Genet. Mol. Biol. 3, 1–25 (2004).

64. Irimia, M. et al. A highly conserved program of neuronal microexons is misregulated in autistic brains. Cell 159, 1511–1523 (2014).

65. Gohr, A. & Irimia, M. Matt: Unix tools for alternative splicing analysis. Bioinforma. Oxf. Engl. 35, 130–132 (2019).

66. Ge, S. X., Jung, D. & Yao, R. ShinyGO: a graphical gene-set enrichment tool for animals and plants. Bioinformatics doi:10.1093/bioinformatics/btz931.

67. Perez-Riverol, Y., et al. The PRIDE database and related tools and resources in 2019: improving support for quantification data. Nucleic Acids Res 47(D1):D442-D450 (2019).

68. McQuin, C. et al. CellProfiler 3.0: Next-generation image processing for biology. PLOS Biol. 16, e2005970 (2018).

69. Rando, O. J., Zhao, K. & Crabtree, G. R. Searching for a function for nuclear actin. Trends Cell Biol. 10, 92–97 (2000).

Acknowledgements:

We thank N. Boni-Kazantzidou (Centre for Proteome Research, Liverpool, UK) and G.-R. Manikas (European Commission, Brussels, Belgium) for the generation of crucial preliminary data; P. Hantzis, M. Fousteri, V. Koliaraki (Institute for Fundamental Biomedical Research, B.S.R.C. “Al. Fleming”) and N. Balatsos (Dept. of Biochemistry and Biotechnology, University of Thessaly, Greece) for cell lines and reagents; D. Black and A. Damianov (Department of Microbiology, Immunology, and Molecular Genetics, UCLA, USA) for plasmids and technical advice on minigene reporter splicing assays; A. Guialis (N.H.R.F., Athens, Greece) for antibodies and reagents; Per Haberkant and the EMBL Proteomics Core Facility for LC-MS/MS analyses and advice; Sofia Grammenoudi and the Flow cytometry facility of B.S.R.C. “Al. Fleming” for help with cell cycle analyses and disussions; Vladimir Benes, Jonathan Landry and the EMBL Genecore for RNA-seq analyses and discussions; Martina Samiotaki, George Stamatakis at the Proteomics Facility of B.S.R.C. “Al. Fleming” for LC-MS/MS analyses and discussions. We also thank George Panayotou and Efthimios Skoulakis (B.S.R.C. “Al. Fleming”) for critical reading of the manuscript; Juan Valcarcel for help with the analysis of the RNA-seq data; Skarlatos G. Dedos (Department of Biology, National and Kapodistrian University of Athens, Greece) for reagents, plasmids, discussions and critical reading of the manuscript.

A.B. was supported by InfrafrontierGR/Phenotypos Infrastructure, co-funded by Greece and the European Union (European Regional Development Fund), under NSRF 2014-2020, MIS 5002135 and by the start-up fund of P.K. M.P. was supported by the start-up fund of P.K. V.P. and Z.E. were supported by the Hellenic Foundation for Research & Innovation (HFRI) and the General Secretariat for Research and Technology (GSRT) to Z.E., under grant agreement 846. J.L. was supported by EMBL Core Facilities. M.R. was supported by the European Research Council (ERC AdvG 670146). M.A. and D.K were supported by InfrafrontierGR/Phenotypos (MIS 5002135). This work was funded by a European Commission Grant FP7-PEOPLE-2010-IEF (274837) to P.K and was supported by a start-up fund to P.K. from a Stavros Niarchos Foundation donation to BSRC "Al. Fleming" and by the Hellenic Foundation for Research & Innovation (HFRI) and the General Secretariat for Research and Technology (GSRT), under grant agreement 846.

Author contributions

These authors contributed equally: Andrada Birladeanu, Malgorzata Rogalska, Myrto Potiri.

A.B. performed most of the immunofluorescence, subcellular fractionation, immunostaining and *in vitro* splicing experiments. M.R. performed all the statistical and bioinformatics analyses. M.P. performed the cellular assays (cell cycle, wound healing, colony formation, MTT assays). Z.E. performed RT-PCR analyses and supervised A.B in *in vitro* splicing assays and M.P in cell cycle analyses and edited the manuscript. V.P. performed immunofluorescence analyses, western blotting analyses, advised A.B. on image acquisition and analyses, supervised M.P. on cellular assays and

edited the manuscript. M.A. and P.K. performed the xenograft experiment. D.K. advised M.A. and helped with the cellular assays. J.D.L. advised and edited the manuscript. P.K conceived, designed and supervised the study, performed the immunoprecipitation experiments and wrote the manuscript. All authors commented on the manuscript.

Competing interests

The authors declare no competing interests.

Materials & Correspondence

Correspondence and material requests should be addressed to P.K.

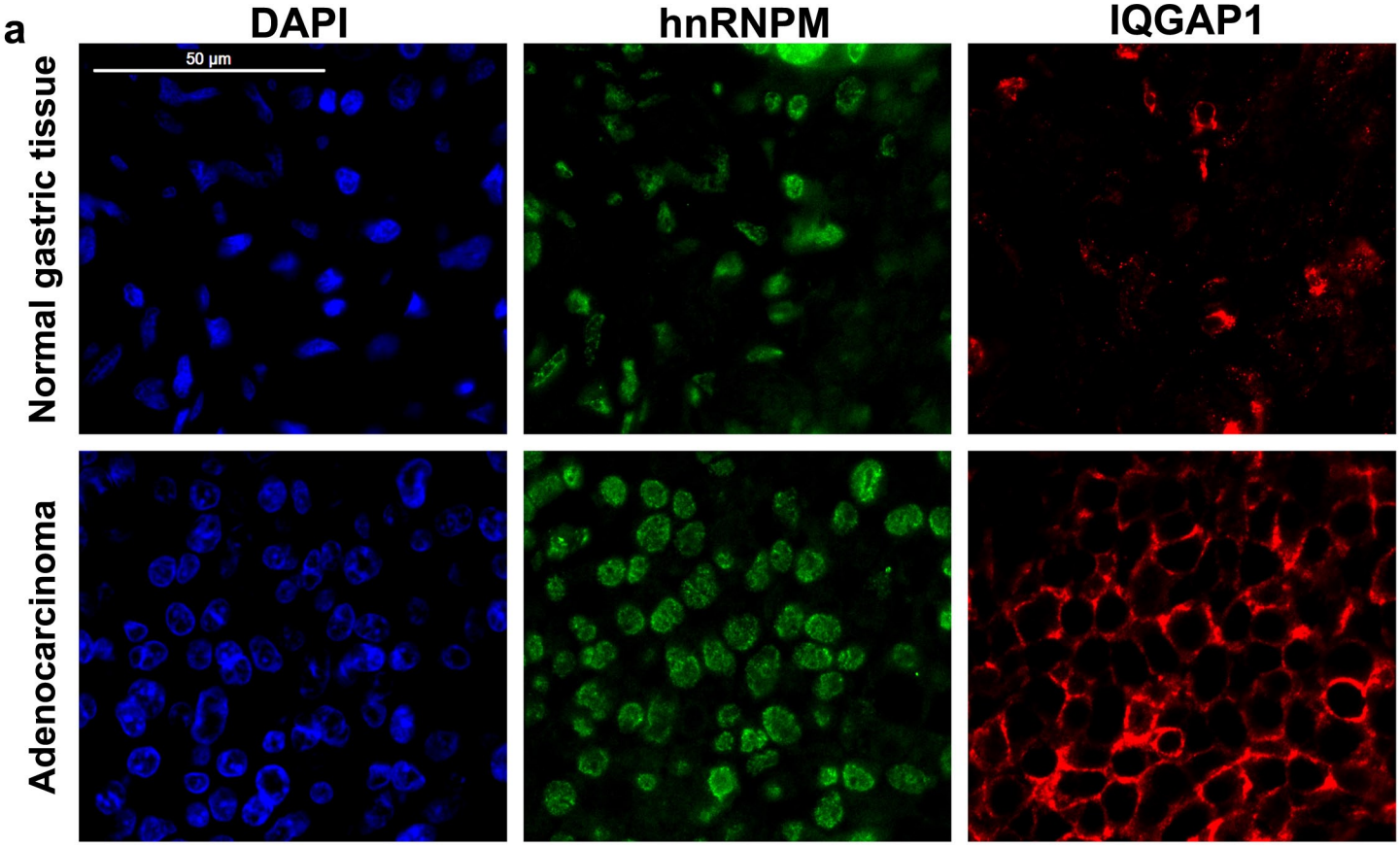
a
DAPI
hnRNPM
IQGAP1
50 μm
Normal gastric tissue
Adenocarcinoma

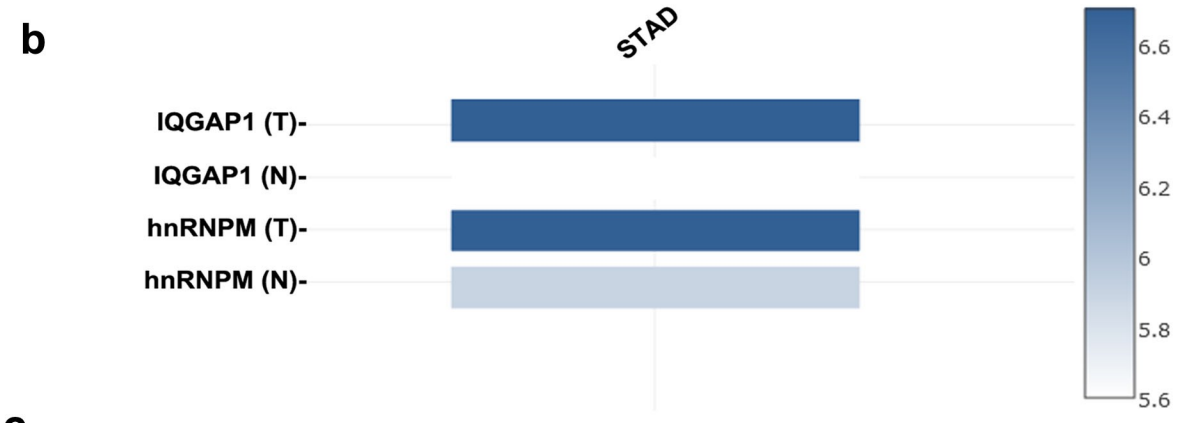
b
STAD
IQGAP1 (T)-
IQGAP1 (N)-
hnRNPM (T)-
hnRNPM (N)-
6.6
6.4
6.2
6
5.8
5.6

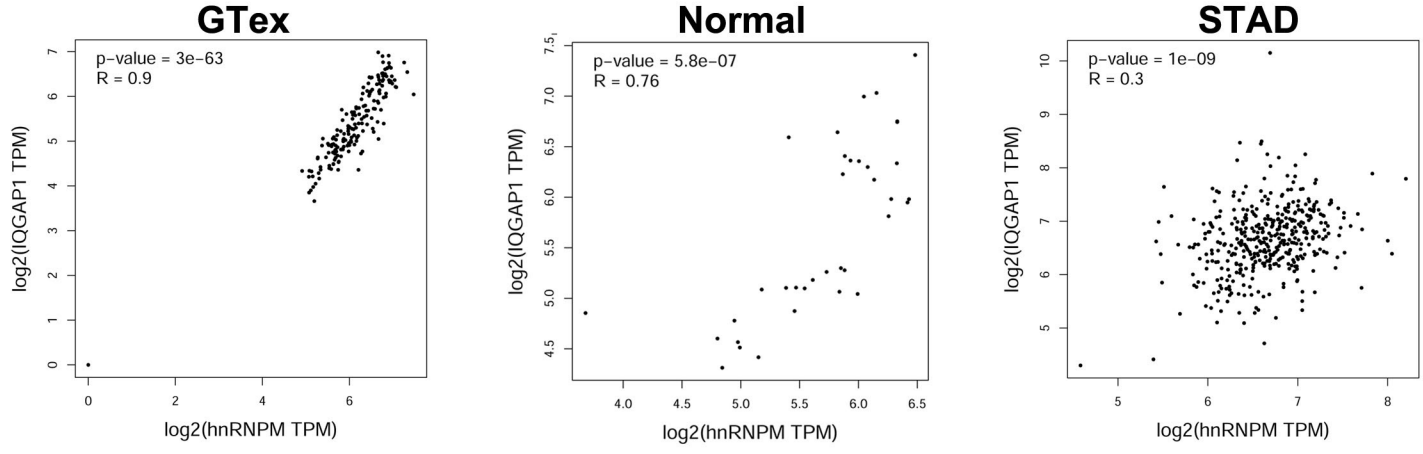
c
GTex
p-value = 3e-63
R = 0.9
log2(IQGAP1 TPM)
log2(hnRNPM TPM)
Normal
p-value = 5.8e-07
R = 0.76
log2(IQGAP1 TPM)
log2(hnRNPM TPM)
STAD
p-value = 1e-09
R = 0.3
log2(IQGAP1 TPM)
log2(hnRNPM TPM)

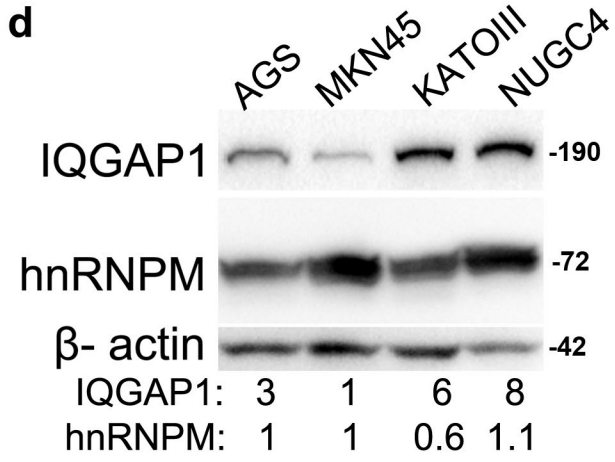
d
AGS
MKN45
KATOIII
NUGC4
IQGAP1
-190
hnRNPM
-72
β- actin
-42
IQGAP1: 3 1 6 8
hnRNPM: 1 1 0.6 1.1

Fig. 1

Fig. 1: hnRNPM and IQGAP1 expression levels are altered in gastric cancer. a Representative epifluorescence images of normal and adenocarcinoma gastric tissues on a commercial tissue microarray. Tissues were immunostained with mouse anti-hnRNPM and rabbit anti-IQGAP1 antibodies. DAPI was used for nuclei staining. The same settings for hnRNPM and IQGAP1 signal acquisition were applied in all samples. **b** Expression matrix plot showing the *IQGAP1* and *HNRNPM* mRNA levels in tumour samples (T) from Stomach Adenocarcinoma (STAD) patients in comparison to TCGA normal and GTex data. The density of colour in each block represents the median expression value of a gene in a given tissue, normalized by the maximum median expression value across all blocks. The expression levels are indicated in $\log_2$(TPM + 1) values. The plot was generated using the gepia2 website (http://gepia2.cancer-pku.cn/#indexn). Sample numbers: 408 tumours, 36 normal and 175 stomach GTex. **c** Correlation plots of the expression of *hnRNPM* and *IQGAP1* mRNAs in normal gastric tissues (GTEx database), normal-adjacent tissues (TCGA STAD Normal database) and tumours from Stomach Adenocarcinoma (STAD) patients (TCGA STAD Tumour database). The plots were generated using the gepia2 website. R: Spearman correlation coefficient. Sample numbers were as in (**b**). **d** Immunoblotting of crude protein extracts from different gastric cancer cell lines against hnRNPM and IQGAP1. β-actin was used to normalize hnRNPM and IQGAP1 levels. MKN45 cells were used as a reference for the comparison of the expression levels between cell lines (ratios shown at the bottom). Quantification was performed using ImageLab software version 5.2 (Bio-Rad Laboratories). AGS: gastric adenocarcinoma; MKN45: poorly differentiated gastric adenocarcinoma, liver metastasis; KATOIII: gastric carcinoma, pleural effusion and supraclavicular and

axillary lymph nodes and Douglas cul-de-sac pleural; NUGC4: poorly differentiated gastric adenocarcinoma, gastric lymph node.

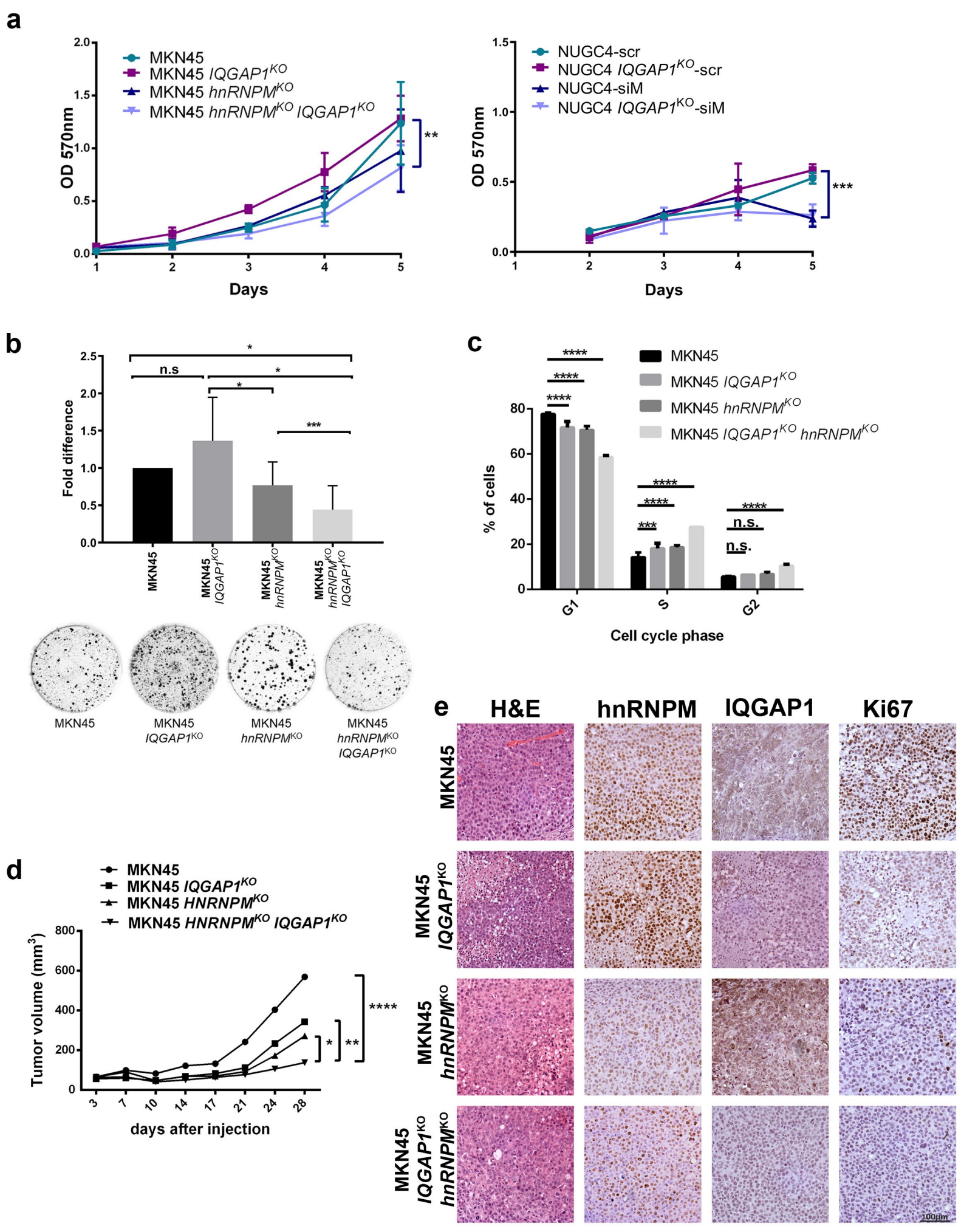
a
MKN45
MKN45 IQGAP1KO
MKN45 hnRNPMKO
MKN45 hnRNPMKO IQGAP1KO
OD 570nm
Days
**
NUGC4-scr
NUGC4 IQGAP1KO-scr
NUGC4-siM
NUGC4 IQGAP1KO-siM
***
b
Fold difference
n.s
*
***
MKN45
MKN45 IQGAP1KO
MKN45 hnRNPMKO
MKN45 hnRNPMKO IQGAP1KO
c
% of cells
****
***
n.s.
G1
S
G2
Cell cycle phase
d
Tumor volume (mm3)
days after injection
****
e
H&E
hnRNPM
IQGAP1
Ki67
100µm

Fig. 2

Fig. 2 hnRNPM and IQGAP1 act co-operatively to regulate tumour growth *in vitro* and *in vivo*. a MTT cell proliferation assays to measure the metabolic activity of gastric cancer cell lines (MKN45, MKN45-*IQGAP1*^{KO}, MKN45-*hnRNPM*^{KO} and double MKN45-*IQGAP1*^{KO}-*hnRNPM*^{KO}, left panel; NUGC4 and NUGC4-*IQGAP1*^{KO} transfected with siRNAs for scrambled control (scr) or hnRNPM (siM); right panel). Growth curves show the mean absorbance values/day from 3 independent experiments. *P* values were calculated using two-tailed, unpaired t-tests, where $^{**}p < 0.01$. **b** 2D colony formation assays to measure the ability of the MKN45-derived cell lines used in (**a**) to form colonies. Bar graph shows the average fold difference ± SD between the numbers of colonies formed across the different groups from 3 independent experiments. *P*-values were calculated using two-tailed, unpaired t-tests, where $^{*}p < 0.05$, $^{***}p < 0.001$. Representative images for each cell line are shown at the bottom. **c** Cell cycle analysis of asynchronous MKN45-derived cell lines using propidium iodide staining followed by FACS analysis. Quantification of the percentage of cells in each cell cycle phase was performed with FlowJo software. Data represent mean values ± SD of two independent experiments. $^{***}p < 0.001$, $^{****}p < 0.0001$. **d** MKN45-derived cell lines were subcutaneously injected into the flanks of NOD/SCID mice and tumours were left to develop over a period of 28 days. The tumour growth graph shows the increase of tumour volume (mm^3) over time. Tumour size was measured in anesthetised mice with a digital caliper twice per week, and at the end-point of the experiment when tumours were excised. Data presented are average values ± SD, from 11 mice per group. *P* values were calculated using one-way ANOVA, where $^{*}p < 0.05$, $^{**}p < 0.01$, $^{****}p < 0.0001$. **e** Excised tumours from all four cell lines were embedded in paraffin, sectioned and stained for H&E and also

probed with antibodies against hnRNPM, IQGAP1 and Ki67. Representative pictures from one tumour from every cell group are shown.

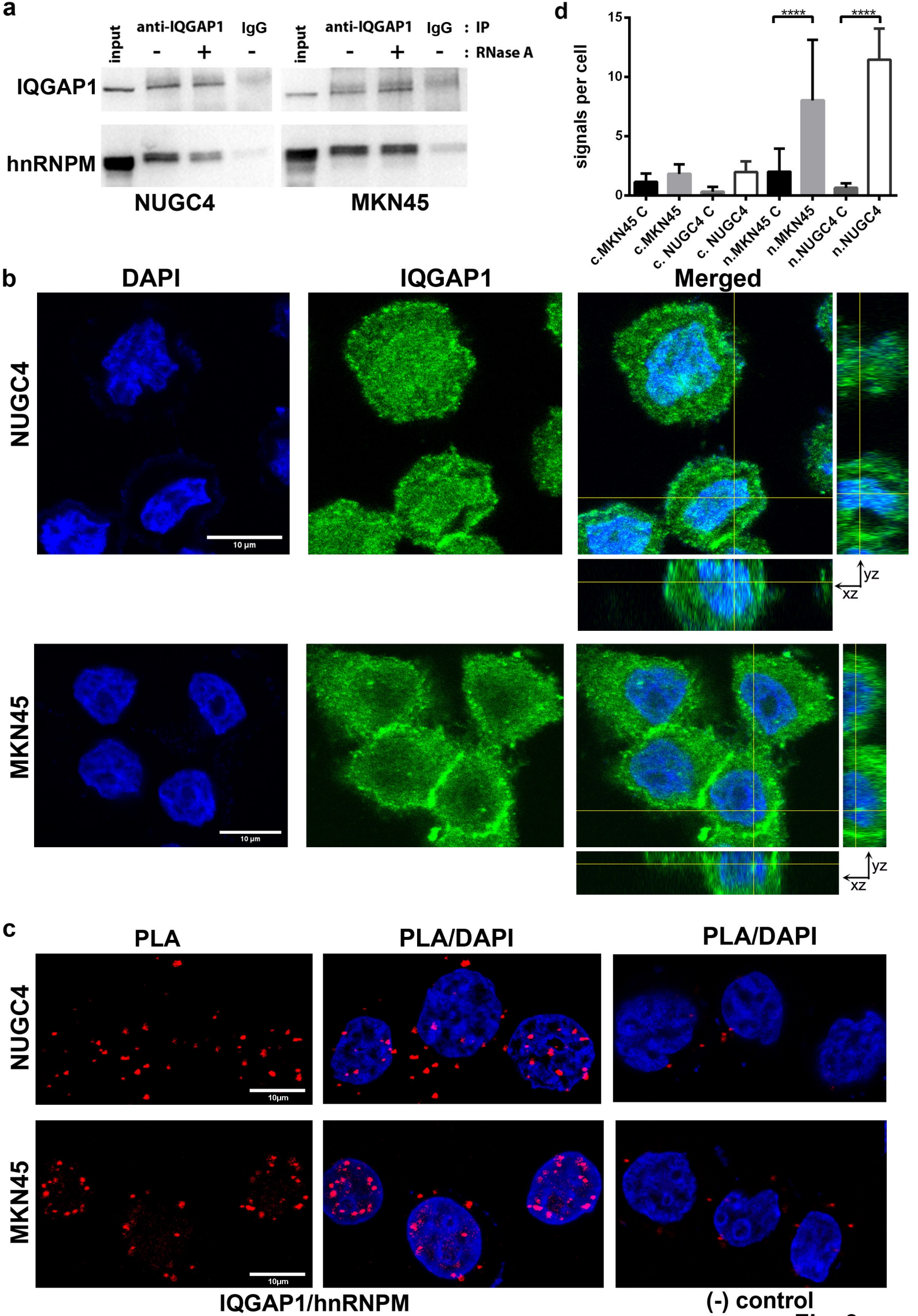
a
input
anti-IQGAP1
IgG
: IP
: RNase A
IQGAP1
hnRNPM
NUGC4
MKN45
d
signals per cell
c.MKN45 C
c.MKN45
c. NUGC4 C
c. NUGC4
n.MKN45 C
n.MKN45
n.NUGC4 C
n.NUGC4
****
b
DAPI
IQGAP1
Merged
NUGC4
MKN45
10 µm
yz
xz
c
PLA
PLA/DAPI
10µm
IQGAP1/hnRNPM
(-) control

Fig. 3

Fig. 3: IQGAP1 and hnRNPM interact in the nucleus of gastric cancer cell lines. **a** Immunoprecipitation with an anti-IQGAP1 antibody or control IgG using nuclear extracts from MKN45 and NUGC4 cells, in the presence or absence of RNase A (0.1 mg/ml for 30 min). Immunoblot detection of IQGAP1 and hnRNPM is shown in comparison to 1/70th of the input used. **b** Representative confocal images of MKN45 and NUGC4 cells stained with an anti-IQGAP1 antibody and DAPI to visualise the nuclei. Single confocal slices are shown for each fluorescence signal and for the merged image. Cross sections of the xz and yz axes show the presence of IQGAP1 within the cell nuclei. **c, d** Proximity ligation assay (PLA) in MKN45 and NUGC4 cells showing the nuclear interaction between hnRNPM and IQGAP1. Representative images for the 2 cell lines displaying a central plane from confocal z-stacks are shown in **(c)**. Negative control (secondary antibody only, MKN45 C and NUGC4 C) samples show minimal background signal. Quantification (**d**) of the nuclear (n.MKN45 and n.NUGC4) and cytoplasmic signal (c.MKN45 and c.NUGC4) was performed per cell, using the DuoLink kit-associated software. Each plot represents at least 15 cells analysed. *P* values were calculated using ANOVA multiple comparisons tests; ****$p < 0.0001$.

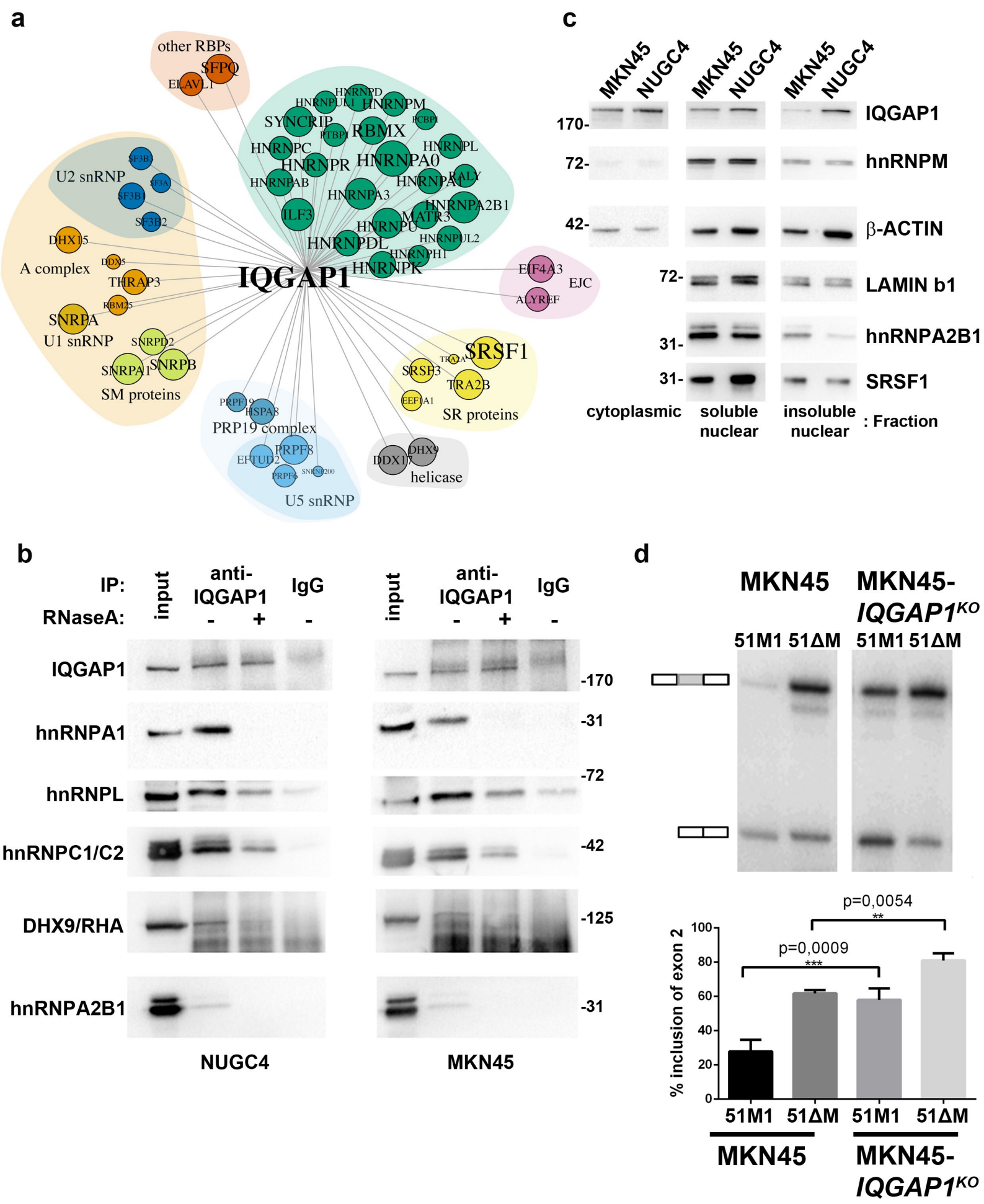
a
other RBPs
SFPQ
ELAVL1
HNRNPD
HNRNPUL1
HNRNPM
SYNCRIP
PCBP1
PTBP1
RBMX
HNRNPC
HNRNPL
HNRNPR
HNRNPA0
RALY
HNRNPAB
HNRNPA1
HNRNPA3
HNRNPA2B1
ILF3
MATR3
HNRNPU
HNRNPUL2
HNRNPDL
HNRNPH1
HNRNPK
IQGAP1
U2 snRNP
SF3B4
SF3A1
SF3B1
SF3B2
DHX15
A complex
DDX5
THRAP3
RBM25
SNRPA
U1 snRNP
SNRPD2
SNRPA1
SNRPB
SM proteins
EIF4A3
EJC
ALYREF
SRSF1
TRA2A
SRSF3
TRA2B
EEF1A1
SR proteins
PRPF19
HSPA8
PRP19 complex
PRPF8
EFTUD2
PRPF6
SNRNP200
U5 snRNP
DHX9
DDX17
helicase
c
MKN45
NUGC4
MKN45
NUGC4
MKN45
NUGC4
170-
IQGAP1
72-
hnRNPM
42-
β-ACTIN
72-
LAMIN b1
31-
hnRNPA2B1
31-
SRSF1
cytoplasmic
soluble nuclear
insoluble nuclear
: Fraction
b
IP:
input
anti-IQGAP1
IgG
RNaseA:
-
+
-
input
anti-IQGAP1
IgG
-
+
-
IQGAP1
hnRNPA1
hnRNPL
hnRNPC1/C2
DHX9/RHA
hnRNPA2B1
-170
-31
-72
-42
-125
-31
NUGC4
MKN45
d
MKN45
MKN45-IQGAP1KO
51M1
51ΔM
51M1
51ΔM
p=0,0054
**
p=0,0009
***
% inclusion of exon 2
100
80
60
40
20
0
51M1
51ΔM
51M1
51ΔM
MKN45
MKN45-IQGAP1KO

Fig. 4

Fig. 4: Nuclear IQGAP1-containing RNPs are involved in splicing regulation. a Network of protein interactions generated from the proteins that were pulled down by anti-IQGAP1 from nuclear extracts of NUGC4 cells classified as spliceosomal components. The network was generated using the igraph R package. Colours represent classes of spliceosomal components according to SpliceosomeDB[28]. Vertices are scaled according to *P* values and ordered according to known spliceosomal complexes. **b** Validation of representative IQGAP1-interacting partners presented in (**a**). Anti-IQGAP1 or control IgG pull down from nuclear extracts of NUGC4 and MKN45 cells were immunoprobed against IQGAP1, hnRNPA1, hnRNPA2/B1, hnRNPC1/C2, hnRNPL and DHX9/RHA. The immunoprecipitated proteins were compared to 1/70th of the input used in the pull down. Where indicated, RNase A was added in the pull down for 30 min. Numbers indicate MW in kDa. **c** Subcellular distribution of hnRNPM and IQGAP1. MKN45 and NUGC4 cells were subjected to subcellular fractionation as described in Methods. Equal amounts of the resulting cytosolic and soluble nuclear fractions as well as the insoluble nuclear material were analysed by Western blot for the presence of IQGAP1, hnRNPM, hnRNPA2/B1 and SRSF1. LAMIN b1 and β-ACTIN were used as fractionation and loading controls, respectively. Numbers indicate MW in kDa. **d** MKN45 and MKN45-*IQGAP1*^{KO} cells were transfected with the DUP51M1 or DUP51ΔM1 minigene splicing reporters[31] for 40 hrs. Exon 2 (grey box) splicing was assessed by RT-PCR using primers located at the flanking exons. Quantification of exon 2 inclusion was performed using ImageJ. Data shown represent the average exon 2 inclusion values ± SD from at least 3 independent experiments. *P* values were calculated using unpaired, two-tailed, unequal variance Student´s t-test.

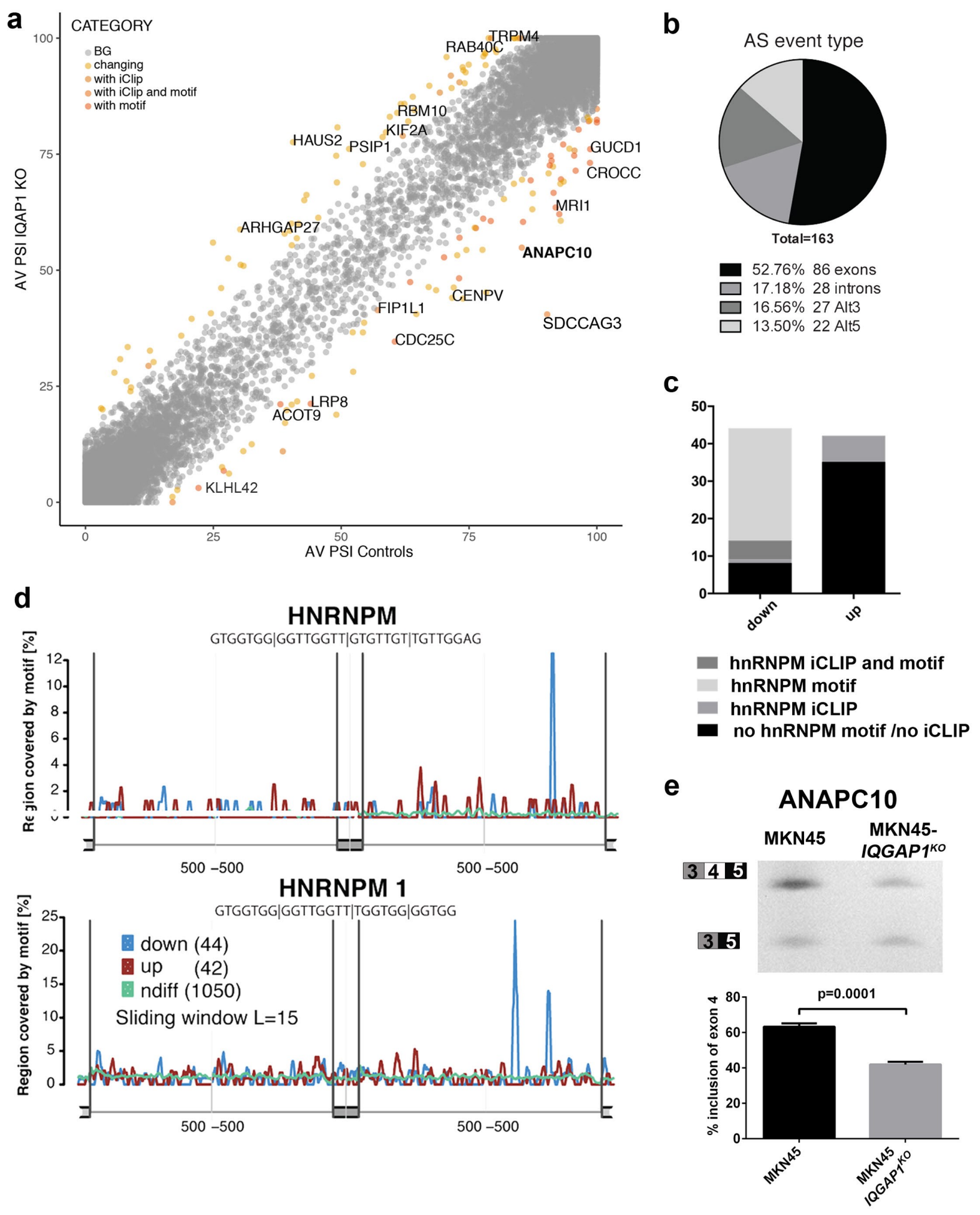
a
CATEGORY
BG
changing
with iClip
with iClip and motif
with motif
AV PSI IQAP1 KO
AV PSI Controls
TRPM4
RAB40C
RBM10
KIF2A
HAUS2
PSIP1
GUCD1
CROCC
MRI1
ARHGAP27
ANAPC10
CENPV
FIP1L1
SDCCAG3
CDC25C
LRP8
ACOT9
KLHL42
b
AS event type
Total=163
52.76% 86 exons
17.18% 28 introns
16.56% 27 Alt3
13.50% 22 Alt5
c
down
up
hnRNPM iCLIP and motif
hnRNPM motif
hnRNPM iCLIP
no hnRNPM motif /no iCLIP
d
HNRNPM
GTGGTGG|GGTTGGTT|GTGTTGT|TGTTGGAG
Region covered by motif [%]
500 –500
HNRNPM 1
GTGGTGG|GGTTGGTT|TGGTGG|GGTGG
down (44)
up (42)
ndiff (1050)
Sliding window L=15
e
ANAPC10
MKN45
MKN45-IQGAP1KO
3 4 5
3 5
p=0.0001
% inclusion of exon 4
MKN45
MKN45 IQGAP1KO

Fig 5

Fig. 5: A broad role of IQGAP1 in hnRNPM-dependent alternative splicing. a Scatterplot with the distribution of the Psi values for the AS events detected by VAST-TOOLS in RNA-seq in IQGAP1^{KO} and control cells. In yellow are the significantly changed AS events between MKN45 and MKN45-IQGAP1^{KO} cells (|ΔPsi|>15, range 5), in ochre and orange are events with detected iClip binding for hnRNPM or predicted RNA-binding motif, respectively. The gene names of the events that were selected for validation are indicated. The ANAPC10 event that was selected for further analysis is shown in bold. BG: background. **b** Pie chart presenting the frequency of the different types of AS events (exon skipping, intron retention, alternative splice donor and alternative splice acceptor) regulated by IQGAP1 in MKN45 cells. **c** Classification of the up-regulated (Up) and down-regulated (Down) exons in MKN45-IQGAP1KO cells compared to MKN45, as i. having the hnRNPM consensus binding motif downstream of the regulated exon, ii. having been identified as iCLIP targets, iii. belonging to both (i.) and (ii.) and iv. not belonging in any of the above categories. **d** Schematic showing the position of the hnRNPM binding motif enrichment relative to the alternatively spliced exon (grey box). The reported hnRNPM motifs[13] were identified only down-stream of the down-regulated exons. **e** IQGAP1^{KO} affects AS of ANAPC10 in MKN45 cells, by promoting exon 4 skipping. RT-PCR (see **Supplementary Table 4**) followed by electrophoresis were used to monitor the rate of *ANAPC10* exon 4 inclusion in MKN45 and MKN45-IQGAP1^{KO} cells. Exon 4 inclusion was quantified with ImageJ in at least 3 biological replicates. *P* value was calculated with unpaired t-test.

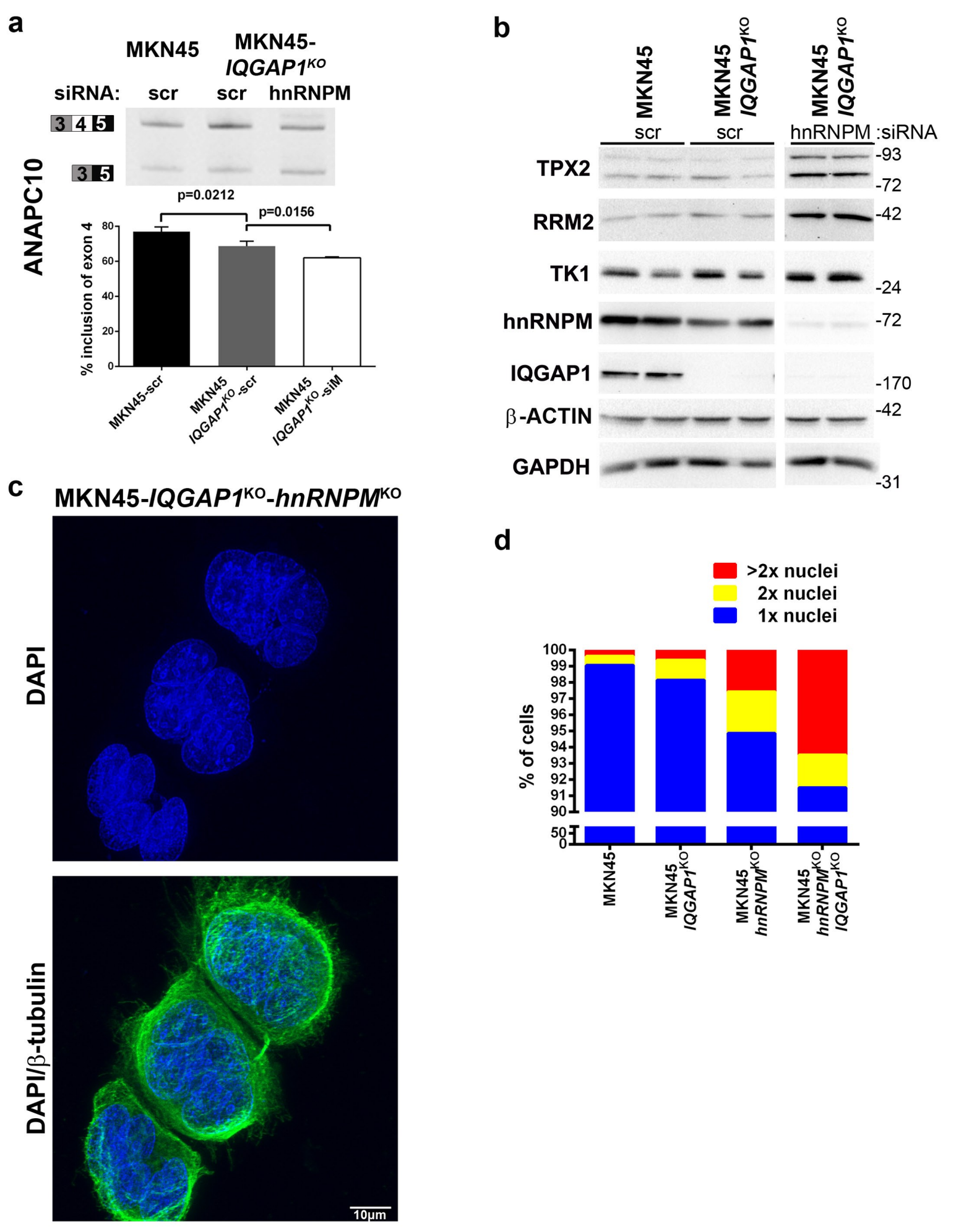
a
MKN45
MKN45-IQGAP1KO
siRNA: scr scr hnRNPM
3 4 5
3 5
ANAPC10
p=0.0212
p=0.0156
% inclusion of exon 4
80
60
40
20
0
MKN45-scr
MKN45 IQGAP1KO -scr
MKN45 IQGAP1KO -siM
b
MKN45 scr
MKN45 IQGAP1KO scr
MKN45 IQGAP1KO hnRNPM :siRNA
TPX2
RRM2
TK1
hnRNPM
IQGAP1
β-ACTIN
GAPDH
-93
-72
-42
-24
-72
-170
-42
-31
c
MKN45-IQGAP1KO-hnRNPMKO
DAPI
DAPI/β-tubulin
10µm
d
>2x nuclei
2x nuclei
1x nuclei
% of cells
100
99
98
97
96
95
94
93
92
91
90
50
0
MKN45
MKN45 IQGAP1KO
MKN45 hnRNPMKO
MKN45 hnRNPMKO IQGAP1KO

Fig 6

Fig. 6: IQGAP1 and hnRNPM co-operatively regulate the function of APC/C through AS of the ANAPC10 pre-mRNA. a *ANAPC10* exon 4 inclusion was analysed in MKN45 and MKN45-IQGAP1^{KO} cells transfected with siRNAs for hnRNPM or scrambled (scr) control siRNAs. RT-PCR (see **Supplementary Table 4**) followed by electrophoresis were used to monitor the rate of ANAPC10 exon 4 inclusion. Exon 4 inclusion was quantified with ImageJ in at least 3 biological replicates. P value was calculated with unpaired t-test. **b** Immunoblot analysis to monitor the steady-state levels of TPX2 (2 isoforms), RRM2 and TK1 in crude protein extracts from MKN45 and MKN45-*IQGAP1*^{KO} cells transfected with siRNAs for hnRNPM or scrambled control (scr) as indicated. *IQGAP1*^{KO} and the efficiency of hnRNPM down-regulation were also confirmed by immunoblotting. β-ACTIN was used as loading control for the TK1 immunoblot and GAPDH was the loading control for all other immunoblots shown. Numbers indicate MW in kDa. **c-d** Non-synchronized cells from all four cell groups were stained for β-tubulin and DAPI, to visualize the cell cytoplasm and nucleus, respectively. A representative confocal image of the double MKN45-*IQGAP1*^{KO}-*hnRNPM*^{KO} stained cells in (**c**) shows the pronounced multi-nucleation observed in these cells. Quantification of the percentage of cells having 1x, 2x or >2x nuclei (**d**) was performed in 20 images from each cell line, reaching a minimum number of 250 cells analysed per group.

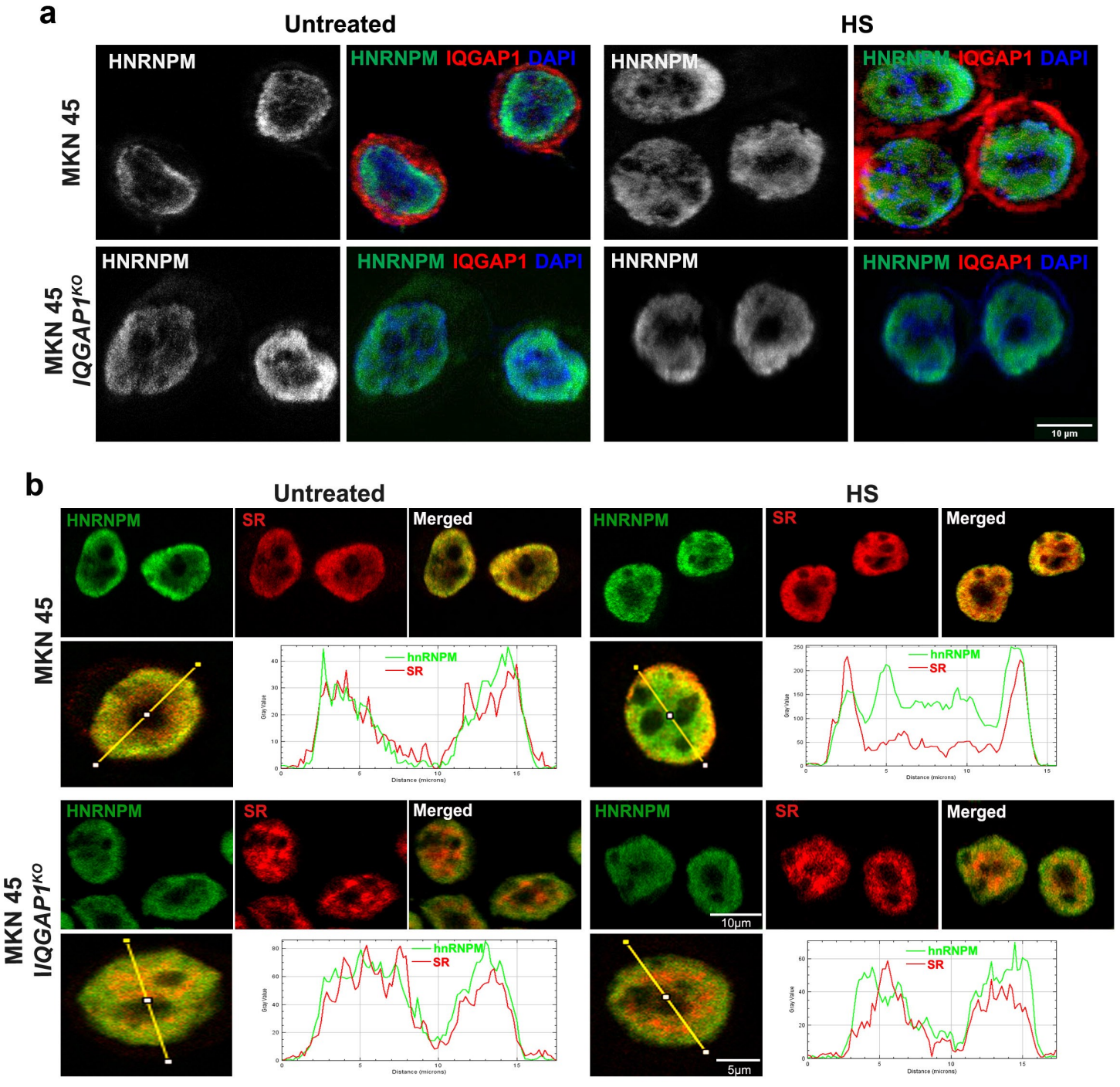
a
Untreated
HS
MKN 45
MKN 45 IQGAP1KO
HNRNPM
HNRNPM IQGAP1 DAPI
10 µm
b
Untreated
HS
MKN 45
MKN 45 IIQGAP1KO
HNRNPM
SR
Merged
hnRNPM
SR
Gray Value
Distance (microns)
10µm
5µm

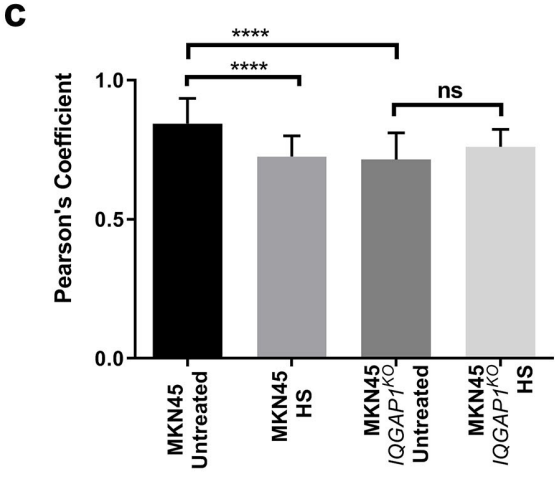
c
Pearson's Coefficient
1.0
0.5
0.0
****
****
ns
MKN45 Untreated
MKN45 HS
MKN45 IQGAP1KO Untreated
MKN45 IQGAP1KO HS

Fig. 7

Fig. 7: IQGAP1 alters hnRNPM's ability to respond to heat-shock by changing its localization relative to SR proteins. a Single confocal planes of MKN45 and MKN45-*IQGAP1*^{KO} cells stained for hnRNPM, IQGAP1 and DAPI after heat-shock (HS) stress induction for 1 hour at 42°C. hnRNPM signal alone is shown in grey for better visualisation and merged images with all three coloured signals are shown on the side. **b** Representative stacks from confocal images of MKN45 and MKN45-*IQGAP1*^{KO} cells stained for hnRNPM and SR proteins. For each condition the single and merged signals of the 2 proteins are shown on top. A single cell stained for hnRNPM and SR is shown on the bottom together with the plot profile line drawn in Image J, while the accompanying pixel grey value graphs are visible on the right of the image. **c** Histogram showing the Pearson's coefficient values for hnRNPM and SR co-localisation, for MKN45 and MKN45-*IQGAP1*^{KO} cells before and after heat-shock stress induction for 1h at 42°C. Pixel-based co-localisation was performed in 36 cells for each of the MKN45 and MKN45-*IQGAP1*^{KO} cells, untreated of after HS, and data represent mean values ± SD. *P* values were calculated using ANOVA multiple comparisons tests; ****$p < 0.0001$.

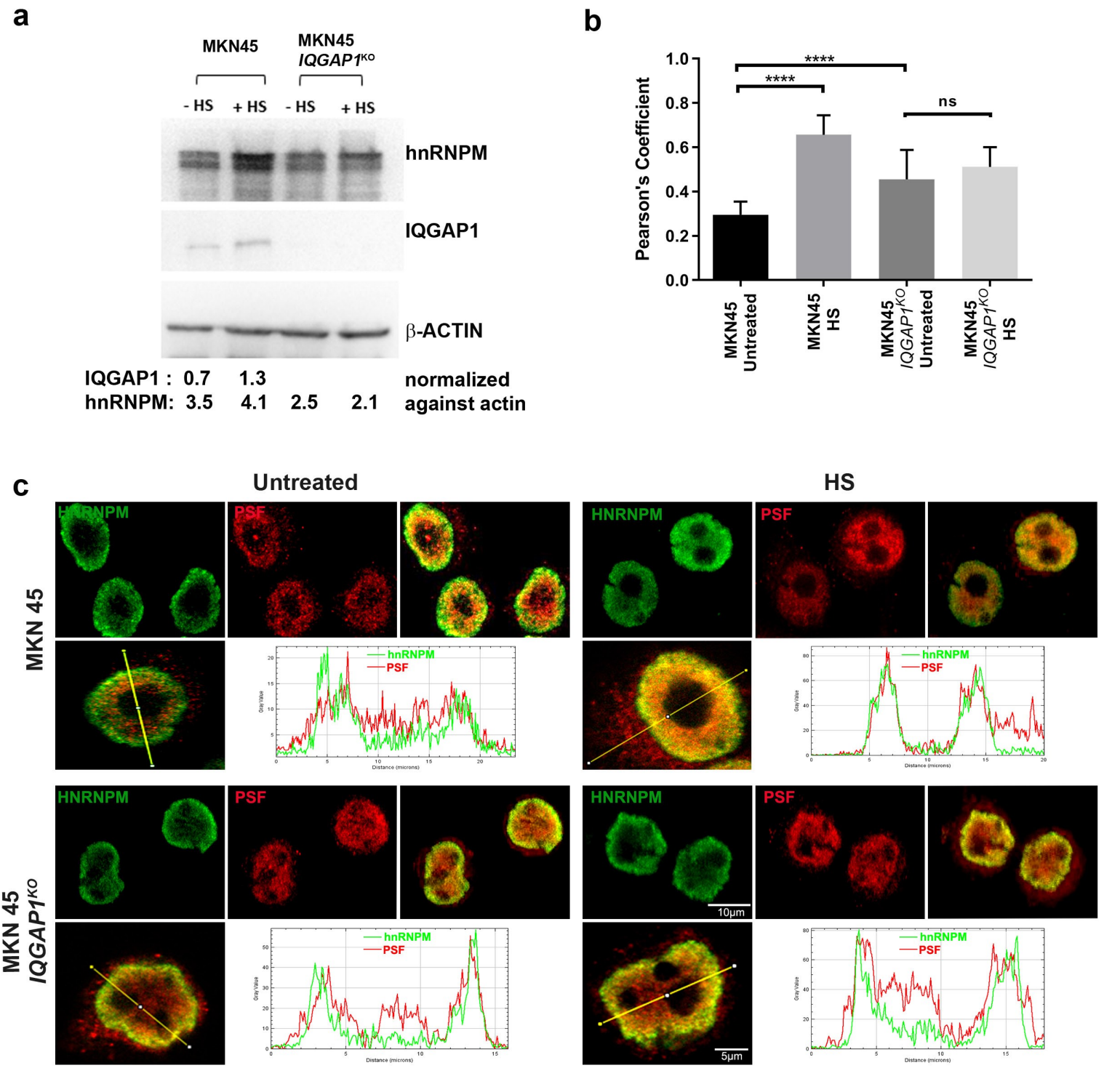
a
MKN45
MKN45 IQGAP1KO
- HS
+ HS
- HS
+ HS
hnRNPM
IQGAP1
β-ACTIN
IQGAP1 : 0.7 1.3
hnRNPM: 3.5 4.1 2.5 2.1
normalized against actin
b
Pearson's Coefficient
1.0
0.8
0.6
0.4
0.2
0.0
****
****
ns
MKN45 Untreated
MKN45 HS
MKN45 IQGAP1KO Untreated
MKN45 IQGAP1KO HS
c
Untreated
HS
MKN 45
MKN 45 IQGAP1KO
HNRNPM
PSF
hnRNPM
PSF
Gray Value
Distance (microns)
10µm
5µm

Fig 8

Fig. 8: IQGAP1 alters hnRNPM's ability to respond to heat-shock by changing its localization relative to SFPQ. a Immunoblot of nuclear matrix extracts from MKN45 and MKN45-*IQGAP1*^{KO} cells before and after heat-shock stress induction for 1hr at 42^{0}C. β-ACTIN is used as a loading control[69]. Quantification of the relevant amounts, in arbitrary units, was performed using ImageLab software version 5.2 (Bio-Rad Laboratories). **b** Pearson's coefficient values for hnRNMP and PSF co-localisation, for MKN45 and MKN45-*IQGAP1*^{KO} cells before and after heat-shock stress induction for 1h at 42°C (exemplar images of cells analysed are shown in c). Pixel-based co-localisation was performed in 30 cells for each of the MKN45 and MKN45-*IQGAP1*^{KO} cells, untreated of after HS, and data represent mean values ± SD. *P* values were calculated using ANOVA multiple comparisons tests; ****$p < 0.0001$. **c** Representative confocal planes of MKN45 and MKN45-*IQGAP1*^{KO} cells stained for hnRNPM and PSF. For each cell type and condition both the single and merged signals of the 2 proteins are shown on top. A slice from a single cell stained for hnRNPM and PSF is visible on the bottom together with the plot profile line drawn in Image J, while the accompanying pixel grey value graphs are shown on the right of the image.

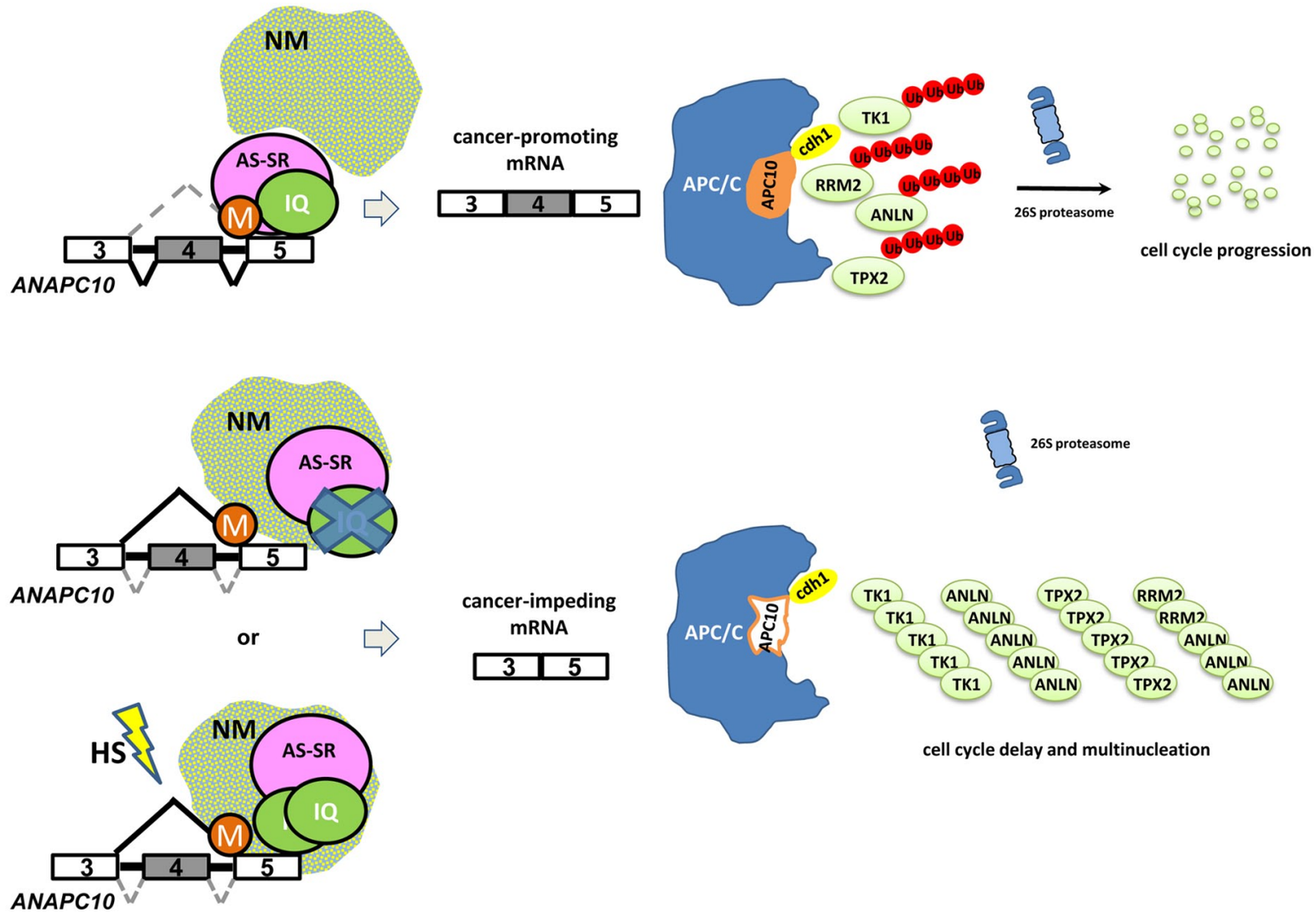

Figure 9

Fig. 9: IQGAP1 regulates hnRNPM-mediated alternative splicing and its response to heat-induced stress. In gastric cancer cells, IQGAP1 (IQ) interacts with hnRNPM (M) and other alternative splicing regulators, such as SR proteins (AS-SR) to promote exon 4 skipping of the *ANAPC10* pre-mRNA. This leads to the formation of a cell cycle-promoting isoform of ANAPC10 that efficiently targets RRM2, TK1, TPX2 and ANLN for degradation. Upon inactivation of IQGAP1, hnRNPM maintains its ability to bind to its pre-mRNA target, but translocates to the nuclear matrix (NM), thus dissociating from the spliceosomal machinery. This favours the formation of a cancer impeding ANAPC10 isoform that recognizes less efficiently RRM2, TK1, TPX2 and ANLN, thus casing their accumulation, cell cycle delay and cell division defects (multinucleation). IQGAP1 responds to heat-induced stress (HS) by translocating to the nucleus, and is required for redistribution of hnRNPM to the nuclear matrix and its dissociation from the spliceosomal machinery.